Temperature Dependence of Acoustic Properties of Natural Snail Mucus by Brillouin Spectroscopy

by

©Dillon Hanlon

A Thesis Submitted in Partial Fulfilment of the Requirements for the Degree of

Master of Science

Department of Physics & Physical Oceanography

Memorial University of Newfoundland

April 2020

St. John's Newfoundland

Abstract

Brillouin light scattering was used to understand how the acoustic and mechanical properties of gastropod mucus are influenced by temperature over the temperature range -11 °C $\leq$ T $\leq$ 52 °C. Two peaks were observed in spectra obtained in this study, one which was present throughout the full temperature range and at a frequency shift of $\sim$ 8.0 GHz, while the other peak appeared at a shift of $\sim$ 18.5 GHz but only for temperatures below ~ -3.0°C. Results for the 8.0 GHz liquid mucus peak showed minor changes in both frequency shift and FWHM for temperatures greater than -2.5 °C. As well, the intensity of this peak showed an overall increase as temperature increases. For temperatures below -2.5°C, the sound velocity for the mucus mode showed an overall increase as temperature decreased, with a difference of $\sim$ 11% between the sound velocity at T = -3.0 °C (1550 m/s) and -11.0 °C (1750 m/s). Moreover, the liquid mucus bulk modulus was also obtained and also shows an overall increase as temperature decreases in this temperature regime. Additionally, this 8.0 GHz peak also revealed an exponential decrease in the FWHM as temperature increased with linewidth ranging from 12 GHz to 0.6 GHz for temperatures T = -11.0 °C and 52.0 °C respectively. Likewise, sound absorption values were also obtained in this study and showed an exponential decrease as temperature increased with values ranging from $\sim 120 \times 10^{-15}$ s^2/m to $\sim 15 \times 10^{-15}$ s^2/m over the temperature range -11 °C $\leq$ T $\leq$ 52 °C for all samples. From the sound absorption, the interaction energy between

the molecules in the mucus was obtained and showed a large change in its values for temperatures above and below T = -2.5 °C. The second peak occurring at $\sim$ 18.5 GHz deemed due to ice I_h showed very small changes in frequency and linewidth as temperature decreases, as well it was seen that as the temperature decreased the intensity of this peak generally increased. The sound velocity for this mode increases slightly as temperature decreases with values ranging from 3800 to 3860 m/s for temperatures T = -3.0 °C and T = -11.0 °C respectively. Likewise, the bulk modulus of the ice slightly increases in this temperature regime. Collectively, the results from this work suggest a phase transition between a viscous liquid state to a mixed solid-liquid state. Comparison of the results obtained in this study is made to similar liquid systems (i.e, water, water and polymer mixtures).

Acknowledgements

First of I would like to thank my supervisor Dr. Todd Andrews for providing me with such an interesting project as well as assisting me in the lab when needed. I would also like to thank Dr. Maynard Clouter for helping me with the design and creation of the variable temperature cell used in this project. As well thanks to Gord Whelan for designing some of the pieces necessary for the temperature cell.

I would like to thank the members of the Andrews research group, Brad and Stephen for your guidance and support throughout this work. As well I'd like to thank my close friends Marisa, and Kyle for your friendship during my MSc program. As well I would like to thank Kaitlyn for your patience and support throughout this project.

Finally I would like to thank my parents for all the support and help you have provided me throughout this project and understanding that I am pursuing something that brings me joy and happiness as well for all the additional help you provide.

Table of Contents

List of Tables

List of Figures

Chapter 1

Introduction

1.1 Gastropod Mucus

The mucus of gastropods (e.g., snails and slugs) is a polymer hydrogel that has a number of roles important for their survival. The polymers of the mucus consist of long chains of glycoproteins that tangle together creating a polymer network [1]. Gastropods produce mucus for two main reasons, (i) lubrication for the purpose of locomotion and (ii) as a defensive mechanism [2]. Depending on whether the mucus is stimulated for either defense or for locomotion, this has an influence on both the composition [3] (i.e, water and glycoprotein concentration) and adhesion, with the composition and adhesion properties being different for each situation [4]. The mucus produced is generally 10 μm to 20 μm thick and depending on the species of gastropod, the mucus can contain anywhere from 91% to 98% of water by weight, with the remaining composition comprising of high molecular weight glycoproteins [5].

1.2 Glycoproteins

Glycoproteins are proteins that have carbohydrates that are linked to amino acid side chains [6] by the process of glycosylation. This is when sugar molecules attach covalently to proteins at nitrogen, oxygen and carbon atoms. [7]. Characteristics of common glycosylated proteins are described in Table 1.1. The types of carbohydrates that are bonded to proteins are known as polysaccharides, which are multiple sugar molecules bonded together [8]. Figure 1.1 shows a simple schematic of a carbohydrate (sugar molecules) linked to an amino acid chain by the process of glycosylation. Glycoproteins of some sort have been found in all organisms studied to date [9, 10].

An interesting property of glycoproteins is their ability to lower the freezing point of liquids such as water, much like antifreeze. This feature resulted in certain glycoproteins being given the name "antifreeze proteins". It turns out that, due to evolutionary changes, a lot of animals (*e.g.*, Atlantic cod) have these proteins in some of their bodily fluids to lower their freezing point in colder climates [11–15].

Table 1.1: Common types of glycosylation that occur with the mechanism that binds sugar to an amino acid chain. An example of organism in which these types of glycosylation is found is also provided.

Type	Description	Organism
N- Linked	Sugar molecules bind to a nitrogen atom of the amino group asparagine.	Humans [16], insects [16] gastropods [17] and plants [18]
O-Linked	Sugar molecules bind to the hydroxyl group of serine or threonine.	Humans [16] and bacteria [19] gastropods [17]
C-Linked	Sugar molecule is added to carbon on the amino acid tryptophan.	Humans [20] and bacteria [21]

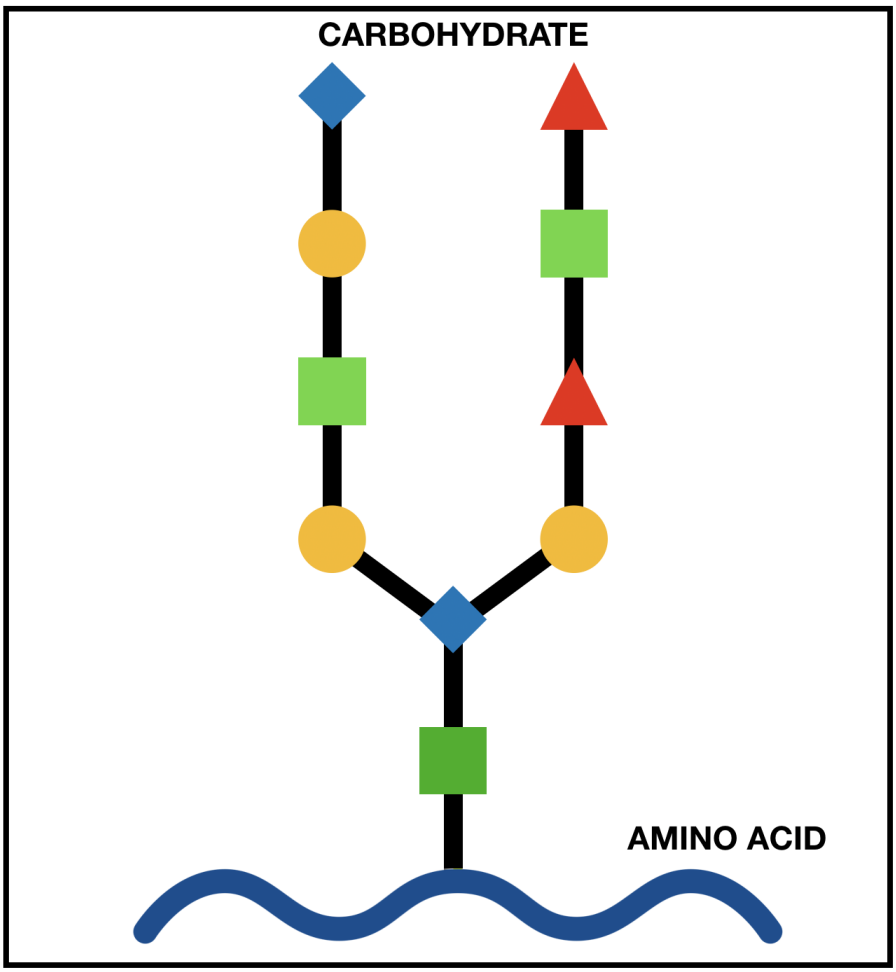

Figure 1.1: A schematic representation of a glycoprotein which has a sugar molecule (carbohydrate) depicted by different shapes linked typically but not exclusively to nitrogen (N), oxygen (O) and carbon (C) which attach the sugar molecules to an amino acid sequence depicted by the blue string.

There are a number of different antifreeze proteins and their properties vary depending on the organism. Thus these proteins are organised into different types based on their characteristic properties. There are two general classifications of antifreeze proteins that either consist of glycoproteins (AFGPs) or nonglycoproteins (AFPs). There are four sub-types of antifreeze proteins (AFPs) labelled Type I - IV. As well the mass of the antifreeze proteins further characterizes the types of these proteins. Antifreeze proteins with the lowest mass are those consisting of glycoproteins (AFGPs), and

the highest mass is an antifreeze protein of Type IV. A complete description of the difference in these proteins has previously been discussed [15]. It has been stated that these antifreeze proteins do not prevent freezing, but rather control the size, and aggregation of ice crystals which ultimately lowers the freezing point of an aqueous solution containing AFGPs [15]. Another characteristic of antifreeze proteins is the ability of a solution composed of a liquid and antifreeze proteins to exhibit thermal hysteresis, a difference between the melting point and the temperature at which ice formation occurs. The rate of cooling of a liquid can influence the thermal hysteresis value of these proteins, thus rapid cooling can decrease the non-equilibrium freezing point [11]. Thermal hysteresis will keep the fluid from freezing. Because of this an organism may have the inability to adapt, and adjust its mucus composition in response to a quick temperature drop [15].

1.3 Previous Studies on Gastropod Mucus

While there have been a few rheological studies of gastropod mucus elasticity, the present work represents the first application of Brillouin light scattering to the study of such mucus and also the first study of the temperature dependence of its elastic properties.

The mechanical properties of *A. columbinus* pedal mucus were studied by measuring the shear tenacity of mucus between two parallel plates under different hydration and strain deformations regimes found in nature [5]. These are *i*) near full hydration and small deformation, *ii*) full hydration and large deformation and *iii*) nearly dry and large deformation. The study by Ref. [5] examines the possibility that the mechanical properties of slug mucus poses limitations on the size and speed of gastropods. First, studies were obtained on fully hydrated mucus ($\sim$ 95 - 97%) at small strains (case *i*).

It was shown that if the mucus is strained sinusoidally with respect to time at low frequencies (< 0.1 Hz), the mechanical properties of the mucus were dominated by its viscosity. However, over a long enough period of time (extremely low frequencies) the mucus behaves as a pure liquid and continues to increase its strain as the period increases. At frequencies on the order of 10 Hz the mucus behaves as a rubbery solid. For case *ii*) the strain abruptly yields and the mucus behaves as a viscous liquid. The yield strength of mucus in this case is dependent on strain rate: the faster the deformation, the stronger the material. This dependence was shown to be described by an exponential function. Similarly, the flow stress of the material increases as a function of strain rate. This study also noted that the transition from liquid to solid in this material is a reversible process. Hence, if the mucus is strained past its yielding point, and behaving as a liquid, and then the strain rate is brought back to zero strain within some small time frame, the molecular network returns back to the original state. As well, deforming the material again will cause the mucus to again behave as an elastic solid. Finally, studies on dried mucus (case *iii*) were performed and it was shown that for hydration values between 97 % and 70 %, the stiffness of mucus varies with hydration and has values ranging from 50 - 150 N/m^2. However, as the hydration drops below 70 %, the modulus increases rapidly until, at the lowest possible hydration at room temperature (10.5 %), the shear modulus is about 5×10^7 N/m^2. Comparing this to hydration values between 70 % and 97 %, the difference is about 200%. This is likely due to the fact that the material is becoming more solid-like below about 70 % hydration. This study also found that when *Littorina aspera* mucus was dried to 0% hydration by being sun baked at 60 °C, it had a modulus of about 9.8×10^8 N/m^2. The reason for the changes in stiffness with dehydration are not known but the authors speculated that it is caused by glycoproteins that interact with water molecules beginning to bond with each other as water is removed. This

bonding increases the crosslinks between glycoprotein chains and as a consequence increases the stiffness modulus. The work by these authors shows how the hydration state can have a major influence on the mechanical properties of gastropod mucus with some aspects still not well understood.

The structure and function of mucus was studied by using a strain gauge force transducer to measure the shear tenacity of mucus in periwinkles (sea snails) and limpets, both marine invertebrates [22]. This study describes the mucus as a dilute polymer network with some solid characteristics but with most of its mass consisting of water. It was also noted in this study that the interactions between polymers cause the mucus to have high stiffness and viscosity. Adhesive gels can be formed via molecules that entangle or crosslink to form a network of polymers. This study also reported that limpet mucus has a wide variation in protein mass, ranging from twenty to two hundred kDa. Limpet mucus also contains two to six times more proteins than carbohydrates. The concentration of glycoproteins in gastropod mucus used for adhesion differs from mucus used in locomotion (trail mucus) by about a factor of two to three. The mucus of periwinkles was also studied and it was found that specific proteins in the mucus make only adhesive bonds. Experiments on the shear tenacity of limpet mucus was conducted by using both trail mucus and adhesive mucus. For the trail mucus the shear tenacity was 2.7 ± 0.3 kPa, whereas the value for adhesive mucus was found to be 190 ± 50 kPa. This comparison shows that the mechanics of the two types of mucus is substantially different. A similar result was obtained for periwinkle mucus. A few of the proposed causes for such changes were *i*) change in the structure of mucus, *ii*) increased adhesion due to the animal clamping down on a surface, and *iii*) increased tenacity due to Stefan adhesion [22–24]. This study also attempted to test the impact of protein concentration in gastropod mucus on the mechanical properties. The results showed a nearly linear increase in normal

tenacity with protein concentration due to either the change in concentration or the change in composition. The cause of this increase is still unknown but it has been noted that the addition of proteins does increase adhesion, but increase in protein concentration alone is not sufficient enough to account for the observed large increase tenacity in actual gastropod mucus [22]. It is mentioned, however, that hydration state does play a crucial role in the stiffness of mucus [5].

The mechanics of gastropod mucus was also studied by performing tensile tests on the mucus of terrestrial slugs, *Arion subfuscus* [25]. It was noted that the mucus of a terrestrial slug has an unusually high stiffness for a gel but retains the high extensibility typical of other mucus. Experiments on unsoaked samples showed stress increased linearly with strain with an average elastic modulus of 30 $\pm$ 5 kPa in the region of low strain. A maximum stress of 101 $\pm$ 15 kPa was achieved at a strain of 3.8 $\pm$ 0.6. After a strain of $\sim$ 5, the stress begins to flatten out with an average stress in this region having a value of 48 $\pm$ 3 kPa. This study stated that freezing and thawing the samples did not have much effect on the mechanical properties. It has been suggested *a priori* that the mucus from gastropods could derive its stiffness from a double network which is composed of a soft network that is the main component of the material, along with a stiff highly cross-linked network. In this suggested arrangment the two interacting networks are composed of glycoproteins which provide the soft network and a network of negatively charged proteins that provide the stiff network. Double networks depend on cross-linked proteins interacting with one another (known as reversible bonds) as opposed to interactions via chemical reactions (covalent bonds). Furthermore, the tensile tests performed in this study provide evidence that the mucus gains its toughness via a double network type mechanism since the results showed a the mucus to be stiff but also showed high extensibility. These two networks would work together to create a much greater toughness and ultimately have two conditions

for maximum toughness which are *i*) that the networks depend on reversible bonds and not covalent bonds, and *ii*) that the two networks are not fully separated. The tensile tests also made the observation that carbohydrates play a much bigger role in the toughness of materials than expected, but the true influence of carbohydrates on mucus toughness is still unknown.

1.4 Previous Studies on Related Liquids

Due to the fact that no previous studies on snail mucus have been performed using Brillouin light scattering and ultrasonics, this section reviews studies of the acoustic properties of the related systems such as solutions of glycerol-water, polyethylene glycol (PEG) and water, polyvinylpyrrolidone (PVP) and water as well as normal and supercooled water and ice I_h. The aqueous solutions of glycerol-water [26], PEG-water [27] and PVP-water [28] will be discussed due to their similar compositions to that of mucus (i.e, mixtures of polymers and water). Normal and supercooled water have been previously studied by Brillouin scattering [29–31] as well by ultrasound [32] and would be a good comparison of work done in this project due to slug mucus mostly consisting of water. As well comparisons to supercooled water and slug mucus below 0 °C are necessary since supercooled water is able to stay in a liquid phase below T = 0 °C similar to slug mucus as discussed later in Chapter 4. Finally, studies on ice I_h will be reviewed here to support the presence of ice crystallites forming in the mucus.

Brillouin scattering has been used to study several samples of polyethylene glycol (PEG) and water mixtures with different concentrations of water [27] over the temperature range 290 K $\leq$ T $\leq$ 380 K. Sound velocities obtained for PEG-water solutions with about $\sim$ 95% water concentration showed that as temperature increased the velocity increased. The sound velocity varied from $\sim$ 1520 m/s at T = 300K to $\sim$

1600 m/s at T = 360K. The magnitude of sound velocity for PEG-water is greater for temperatures above T = 0°C than the sound velocity of water in this same temperature region. Both the sound absorption for PEG-water and pure water showed that as the temperature is increased, the sound absorption decreases. These results are consistent with what has previously been seen for the sound absorption in water [29]. The values of sound absorption for PEG-water at T = 300K and 360K were found to be 40 $\times 10^{-15}$ s^2/m to 20 $\times 10^{-15}$ s^2/m, respectively.

The sound velocity and sound absorption of polyvinylpyrrolidone (PVP) and water solutions as a function of temperature has been studied using ultrasound [28] over the range 20°C $\leq$ T $\leq$ 45°C. For concentrations of 5% PVP and 95% water the sound velocity increased as temperature increased. The sound velocity varied from 1510 m/s at T = 0°C to 1560 m/s at T = 45°C. Likewise, the sound absorption showed a nonlinear decrease in sound absorption as temperature increased. Values obtained in this study ranged from 55 $\times 10^{-15}$ s^2/m at T = 20°C and 35 $\times 10^{-15}$ s^2/m at T = 45°C. The overall trends for the sound velocity and sound absorption are consistent with other aqueous solutions previously studied [27]. As well, the results from this work show similarities in both the sound velocity and sound absorption to what has previously been reported for water [29–32] in the sense that all studies show a general increase in velocity and decrease in sound absorption as temperature increases.

Brillouin scattering was used to measure the sound velocity and sound absorption in normal and supercooled water over the temperature range -10°C $\leq$ T $\leq$ 10°C [29]. The results obtained in that experiment showed a linear temperature dependence increase in sound velocity with values obtained ranging from 1390 m/s at T = 0 °C to 1550 m/s at T = 70 °C. For temperatures greater than 70 °C the sound velocity begins to plateau until about 90 °C after which the velocity slightly decreases. In the supercooled regime T $\leq$ 0 °C, the sound velocity decreases rapidly at a rate of -11.0

m/s/°C. Studies on sound absorption as a function of temperature were also obtained in this work and showed that the damping of sound waves displayed a maximum damping of 70 $\times 10^{-17}$ s^2/cm at T = -10°C. This work also showed the temperature dependence of sound absorption decreased exponentially as temperature increased with the lowest value being 5 $\times 10^{-17}$ s^2/cm at T = 70 °C. The sound velocity of water was also obtained from Brillouin scattering as a function of temperature over the range 0°C $\leq$ T $\leq$ 50 °C [31]. Results showed the sound velocity varied from $\sim$ 1400 m/s at T = 0 °C to 1540 m/s at T = 50 °C. Results are consistent with previous studies on water for this temperature range [29, 30].

Similarly, Brillouin scattering was also used to obtain sound velocity and sound absorption measurements on normal and supercooled water over the temperature range -20°C $\leq$ T $\leq$ 20°C [30]. A large change in sound velocity was observed with a minimum velocity of about 1250 m/s at T = -20°C and a maximum of approximately 1470 m/s at T = 20°C, which is consistent with previous results for water [29]. Sound absorption showed a maximum value of 120 $\times 10^{-15} s^2/m$ at T = -20°C and exponentially decreased to 20 $\times 10^{-15} s^2/m$ at T = 20°C. Both sound velocity and sound absorption obtained for water in this study are consistent with previous results on water [29,31,32] as well with results obtained for polyethylene glycol-water mixture [27]. These studies all show that as temperature increases, the sound absorption decreases.

The temperature dependence of sound absorption of ultrasonic waves in water was obtained for temperatures in the range 0°C $\leq$ T $\leq$ 33°C [32]. Results showed an exponential decrease as temperature increased. Values ranged from 137 $\times 10^{-15}$ s^2/m at T = 0°C and 40$\times 10^{-15}$ s^2/m at T = 33°C. These results are quite different from the sound absorption values previously obtained by Brillouin scattering [29,30]. Values of sound absorption for water obtained by ultrasonic waves are approximately 3 times the values obtained by Brillouin scattering at T = 0 °C and T = 30 °C [29, 30]. The

difference between the sound absorption obtained by the two methods, may suggest that the sound absorption is sensitive to one method over the other.

Ultrasound was also used to study the temperature dependence of sound absorption in an aqueous solution of glycerol in water [26] over the range 30°C $\leq$ T $\leq$ 60°C. Results showed that for a concentration of 15% glycerol and 85% water the sound absorption increases slightly from $\sim$ 300 $\times 10^{-15} s^2/m$ at T = 25°C to $\sim$ 600 $\times 10^{-15} s^2/m$ at T = 60°C. This increase in sound absorption as temperature increases is unlike what has been observed in previous studies on other polymer and aqueous solutions [27, 28]. As well, this behaviour is different than that of water [29, 31, 32]. The overall magnitude of the sound absorption in a glycerol-water mixture is about 10 times bigger than for previous studies on water, and solutions of PEG-water and PVP-water [27–30].

Brillouin spectroscopy on ice including I_h was performed at a temperature of T = -35.5°C [33]. The longitudinal velocity of ice I_h was reported having a value of $\sim$ 3900 m/s. The bulk modulus for this ice I_h mode was obtained and reported having a value of 9.24 GPa. Likewise, Brillouin scattering on several samples of ice I_h at temperatures were studied [34, 35] and the velocity for the longitudinal mode of ice I_h was reported to have values of 3750 m/s at T = -3.0°C and 3830 m/s at T = -16.0°C [34, 35]. The bulk modulus for ice I_h was also reported having a value of 8.89 GPa in Ref. [35] at T = -16.0°C and. This value is within $\sim$ 10% to the value previously reported for ice I_h [33]. The values reported for ice are comparable throughout each study, and values are expected to be slightly different for different temperatures.

As can be seen from the previous studies discussed throughout this chapter, the sound velocity of related liquids increases with decreasing temperature, whereas the sound absorption decreases with increasing temperature. This behaviour is consistent in both studies that use Brillouin scattering [28–30] as well as the studies that use

ultrasonics [32]. However, it is surprising that the temperature dependence study on glycerol by ultrasonics show that the sound absorption increases with increasing temperature [26]. One possible cause of this difference could due to the fact that the glycerol to water concentration was higher than the previous polymers to water studies. Based on these results, it should be expected that a similar trend is expected for slug mucus as a function of temperature.

1.5 Motivation

As was mentioned earlier in this chapter, the temperature dependence of the elastic properties of gastropod mucus has not been investigated. In this study, Brillouin spectroscopy was used to probe this dependence and also to characterize the nature of a previously unknown phase transition in this system. In doing so, this work contributes to our understanding of nucleation in biological systems and further demonstrates the capabilities of Brillouin scattering in the study of natural materials.

In addition to the scientific motivation mentioned above, slug mucus has gained a lot of attention in recent years due to its possible applications in medicine [36]. Research is being done to try and understand how to effectively create non-toxic, medical adhesives that could replace typical sutures currently being used in medicine. Slug mucus has the ability to adhere to wet surfaces which is very interesting and shows promise to replace sutures being used to close wounds inside the human body [36]. Characterization of the elastic properties and how they vary with temperature, especially over the normal body temperature range, will certainly be important in the development of such applications.

1.6 Scope

This thesis presents the results of a study on the temperature dependence of the elastic properties of gastropod mucus by Brillouin spectroscopy. Chapter 1 provides an introduction to gastropod mucus and reviews previous studies on related systems such as water, mixtures of water and polyethylene glycol, glycerol-water, and polyvinylpyrrolidone-water as well as ice I_h. Chapter 2 reviews Brillouin scattering theory and the quantities (sound velocity, sound absorption and bulk modulus) that can be obtained from Brillouin spectra. Chapter 3 describes the apparatus, including the heating and cooling system and the optical setup. Chapter 4 presents the results obtained in this work and comparisons to the findings of previous studies on related systems. Finally, Chapter 5 summarizes the results obtained in this work.

Chapter 2

Theory

2.1 Theory of Brillouin Scattering

In order to understand Brillouin scattering in liquids, the underlying theory behind Brillouin scattering will first be outlined. Both the classical and quantum mechanical approaches to Brillouin scattering will be discussed, leading to an equation relating frequency shift and acoustic phonon velocity. Later in this chapter a derivation of Brillouin scattering in liquids will be presented and from this derivation a relationship between the spectral line shape, phonon velocity and frequency shift will yield information about sound absorption of phonon modes. As well, the theory behind the mechanical properties of liquids will be presented in this chapter.

2.1.1 Classical Theory

In the classical theory of thermal scattering for temperatures $T \geq 0K$, a medium is treated as if elastic waves of all frequencies were passing through it in all directions and its internal structure is disregarded [37]. The frequency shift of light incident on a medium can be derived by considering the interaction between a light wave with

frequency f_i and wavelength λ_i and a mechanical plane wave travelling in a medium with frequency f_s. These plane waves can be represented by regions of higher and lower densities as depicted in Fig 2.1. Constructive interference of light occurs when the Bragg condition

$$\lambda_i = 2nd\cos\phi$$

where d is the distance between planes and ϕ is the angle of incidence, is satisfied. It should be noted that, since the angle of incidence must equal the angle of reflection, the scattering angle θ then becomes $\theta = \pi - 2\phi$ so that the Bragg condition becomes

$$\lambda_i = 2nd\sin\frac{\theta}{2} = 2n\lambda_s\sin\frac{\theta}{2}. \tag{2.1}$$

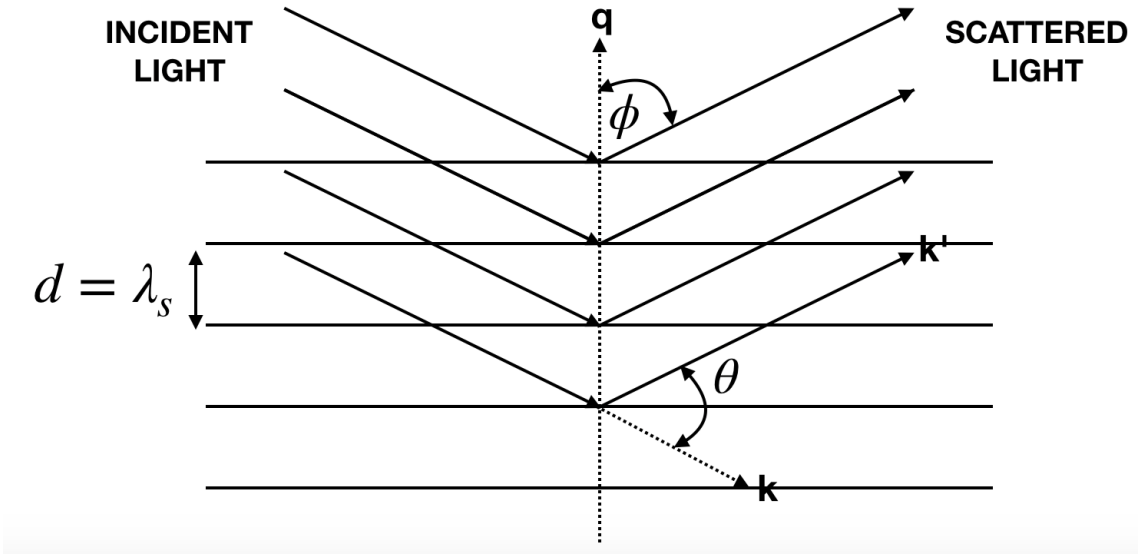

Figure 2.1: Schematic of scattering due to a Bragg reflection off thermally excited sound waves.

If the planes in Fig 2.1 are now moving with a velocity $\vec{v}$ then the scattered light is

Doppler-shifted by an amount,

$$f = \pm \frac{2 f_i v n}{c} \sin \frac{\theta}{2} \tag{2.2}$$

where c is the speed of light in vacuum and n is the refractive index of the medium. Eqn 2.2 is the well known Brillouin equation presented by Leon Brillouin in 1922 [38]. It should be noted that for a 180° backscattering geometry, like that used in the present work, then $\theta = 180°$.

2.1.2 Quantum Theory

Brillouin scattering can also be described quantum mechanically by considering the interaction between an incident photon and a medium resulting in the creation or annihilation of an acoustic phonon as shown schematically in Fig 2.2.

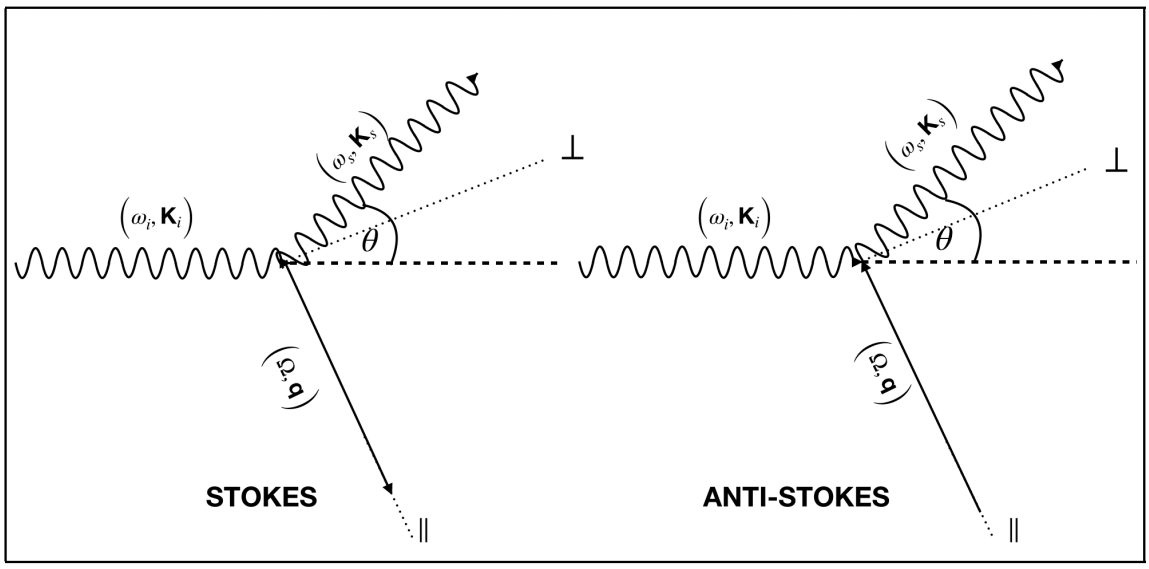

Figure 2.2: Schematic of the process of creation (Stokes) and annihilation (anti-Stokes) of a phonon in the process of light scattering. ω, $\mathbf{K}$ - frequency and wave vector of incident and scattered light. Ω, $\mathbf{q}$ - frequency and wave vector of the phonon.

For this scattering process, conservation of energy and momentum yield

$$\hbar\omega_s = \hbar\omega_i \pm \hbar\Omega \tag{2.3}$$

and

$$\hbar\mathbf{K}_s = \hbar\mathbf{K}_i \pm \hbar\mathbf{q} \tag{2.4}$$

where the indices i and s represent incident and scattered light, respectively. As well, ω and $\mathbf{K}$ are the frequency and wavevector of light, respectively and Ω and $\mathbf{q}$ are the frequency of the phonon and wavevector of the phonon, respectively.

It is now possible to write Eqn 2.4 in component form where the components are parallel and perpendicular to the phonon propagation as shown in Fig 2.2. The components of the wavevector for the scattered light are then

$$K_{s\parallel} = K_{i\parallel} \pm q_{\parallel} \tag{2.5}$$

and

$$K_{s\perp} = K_{i\perp} \pm q_{\perp} \tag{2.6}$$

From the geometry shown in Fig 2.2 we see that $q_\perp = 0$ and $q_\parallel = q$. Also since the frequency shift of Brillouin scattering is much less than that of the incident (scattered) light it is possible to use the approximation $K_s \approx K_i$, and then rearranging Eqn 2.5 yields,

$$K_i \sin(-\frac{\theta}{2}) = K_i \sin(\frac{\theta}{2}) \pm q \tag{2.7}$$

where $\theta/2$ comes from the geometry of Fig 2.2.

The magnitude of the phonon wavevector q can then be written as,

$$q = 2nK_i \sin(\frac{\theta}{2}). \tag{2.8}$$

Now using the following relations,

$$f_s = \frac{vq}{2\pi} \tag{2.9}$$

and

$$f_i = \frac{cK_i}{2\pi} \tag{2.10}$$

it is now possible to write Eqn 2.8 as,

$$f = \frac{2f_i nv}{c} \sin\frac{\theta}{2} \tag{2.11}$$

which is equivalent to the result obtained previously in the classical derivation. Again, $\theta = 180^\circ$ for the backscattering geometry used here.

2.2 Brillouin Scattering in Liquids

In order to obtain more information on the scattering process we must now extend the derivations to the classical theory of scattering. First we begin by allowing the electric field of incident light to have the plane wave form of

$$E_i(\vec{r}, t) = E_0 \exp[i(\mathbf{k}\cdot\vec{r} - \omega_0 t)] \tag{2.12}$$

as represented in Fig 2.3. The incident light wave produces an oscillating polarization $\mathbf{P}(\vec{r}, t)$ in the medium. This polarization in the infinitesimal volume $|d\vec{r}|$ radiates an

electric field whose value at the field point $\vec{R}$ is given by

$$d\vec{E}_s(\vec{R},t) = \frac{\frac{d^2}{dt^2}\mathbf{P}(\vec{r},t-\frac{|\vec{R}-\vec{r}|}{c})\sin\phi|d\vec{r}|}{c^2|\vec{R}-\vec{r}|} \tag{2.13}$$

where ϕ is the angle between incident $\vec{E}_i$ and and wave vector k' of the scattered light wave (not shown in Fig 2.3) [39].

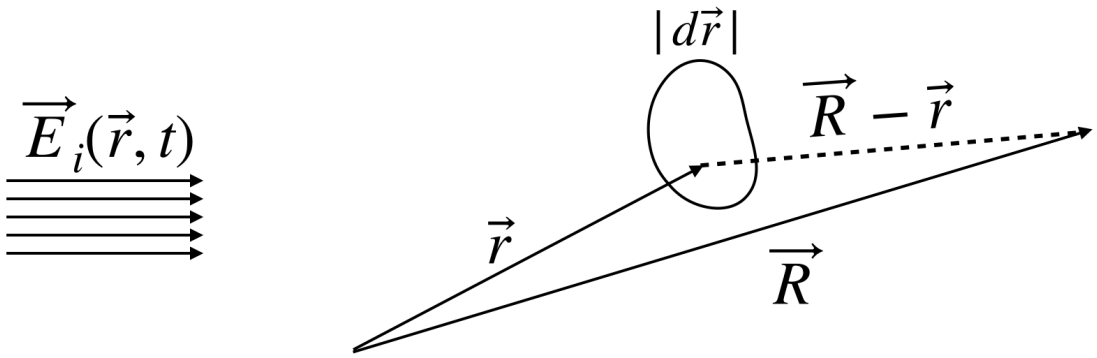

Figure 2.3: Schematic of an incident wave $\vec{E}_i$ incident on a medium with volume element $|\mathrm{d}\vec{r}|$ where $\vec{r}$ is the source point and $\vec{R}$ is the field point.

Recall that the polarization $\mathbf{P}(\vec{r},t)$ is related to the incident field via the electric polarizability $\alpha(\vec{r},t)$ which can be written as

$$\mathbf{P}(\vec{r},t) = \alpha(\vec{r},t)\vec{E}_i(\vec{r},t). \tag{2.14}$$

where,

$$\alpha(\vec{r},t) = \frac{\varepsilon(\vec{r},t)-1}{4\pi}$$

In the presence of thermally excited sound waves, both α and ε (dielectric constant) are functions of both position $\vec{r}$ and time t [39].

It is now possible to calculate the second derivative of $\mathbf{P}(\vec{r},t)$ with respect to time (as required by Eqn. 2.13). If $\vec{R} \gg \vec{r}$ then by integrating over the illuminated volume,

Eqn. 2.13 the electric field at $\vec{R}$ becomes [39],

$$\vec{E}_s(\vec{R},t) \cong E_0(\frac{\omega_0}{c})^2 \frac{\exp[i(\mathbf{k}\cdot\vec{R}-\omega_0 t)]\sin\phi}{\vec{R}} \cdot \int_V \alpha(\vec{r},t)\exp[i(\mathbf{k}-\mathbf{k}')\cdot\vec{r}]|d\vec{r}| \quad (2.15)$$

where $\mathbf{k}' = 2\pi/(\lambda_i/n)$ and where V is the volume illuminated by the incident wave. Thus, the scattered field is a spherical spreading wave whose amplitude is determined by the interference integral which is the last term in Eqn. 2.15.

$$I = \int_V \alpha(\vec{r},t)\exp[-i(\mathbf{q}\cdot\vec{r})]|d\vec{r}| \quad (2.16)$$

where $\mathbf{q} = \mathbf{k}' - \mathbf{k}$ from Fig 2.1. The interference integral represents the superposition having different phases of waves, scattered from all points in the medium [39]. The polarizability can be written in terms of its average and fluctuations about the average such as

$$\alpha(\vec{r},t) = \langle\alpha\rangle + \delta\alpha(\vec{r},t) \quad (2.17)$$

where $\langle\alpha\rangle$ and $\delta\alpha(\vec{r},t)$ are the average polarizability and fluctuations about the average, respectively. Upon substitution of Eqn. 2.17 into Eqn. 2.16 one obtains

$$I = \int_V \langle\alpha\rangle\cdot\exp[-i(\mathbf{q}\cdot\vec{r})]|d\vec{r}| + \int_V \delta\alpha(\vec{r},t)\exp[-i(\mathbf{q}\cdot\vec{r})]|d\vec{r}|$$

and since the average polarizability $\langle\alpha\rangle$ term in the integral does not depend on $\vec{r}$, the volume integral in the first term will produce scattering only in the forward direction $\mathbf{q} = 0$ [39]. This means scattering in any other direction is caused purely from the fluctuation term $\delta\alpha(\vec{r},t)$. In order to evaluate this term the fluctuations are written terms of Fourier components,

$$\delta\alpha(\vec{r},t) = \frac{1}{(2\pi)^{3/2}}\int|d\vec{q}|\exp[i\vec{q}\cdot\vec{r}]\delta\alpha(\vec{q},t) \quad (2.18)$$

where $\vec{q}$ on the right hand side is just a variable used for a Fourier transformation. Substitution of Eqn. 2.18 into Eqn 2.16 then yields

$$I = \frac{1}{(2\pi^{3/2})} \int \mid d\vec{q} \mid \delta\alpha(\vec{q}, t) \int_V \exp[i(\vec{q} - \mathbf{q}) \cdot \vec{r}] |d\vec{r}| \tag{2.19}$$

however the last term in Eqn.2.19 is the Dirac delta function,

$$\int \exp[i(\vec{q} - \mathbf{q}) \cdot \vec{r}] |d\vec{r}| = (2\pi)^3 \delta(\vec{q} - \mathbf{q}) \tag{2.20}$$

which is zero unless $\vec{q} = \mathbf{q}$.

It is now possible to write a formula for the scattered field using Eqn 2.20, 2.19, 2.15 and $\delta\alpha = \delta\varepsilon/4\pi$, the result is

$$\vec{E}_s(\vec{R}, t) = E_0 \Big(\frac{\omega_0}{c}\Big)^2 \frac{\sin\phi}{4\pi} \frac{\exp[i(\mathbf{k} \cdot \vec{R} - \omega_0 t)]}{\vec{R}} (2\pi)^{3/2} \delta\varepsilon(\mathbf{q}, t) \tag{2.21}$$

where the term $\delta\varepsilon(\mathbf{q}, t)$ is given by [39],

$$\delta\varepsilon(\mathbf{q}, t) = \frac{1}{(2\pi)^{3/2}} \int |d\vec{r}| \exp[-i\mathbf{q} \cdot \vec{r}] \delta\varepsilon(\vec{r}, t) \tag{2.22}$$

To find the spectrum and intensity of scattered light we use the fact that the spectral density of $E_s^2(\vec{R}, t)$ is the Fourier transform of the correlation function of the scattered field. The correlation function of the electric field R_E, is a function of the correlation time τ and is defined by [39],

$$\begin{aligned} R_E(\tau) &= \langle \vec{E}_s(\vec{R}, t + \tau) \cdot \vec{E}_S^*(\vec{R}, t) \rangle \\ &= \lim_{\tau \to \infty} \frac{1}{2T} \int_{-T}^{T} \vec{E}_s(\vec{R}, t + \tau) \cdot \vec{E}_S^*(\vec{R}, t) dt, \end{aligned} \tag{2.23}$$

which has the property that when $\tau < 0$ then $R_E(\tau) = 0$ [40]. The spectral density

of the scattered radiation $S(\mathbf{q},\omega)$ is given by,

$$S(\mathbf{q},\omega) = \frac{1}{2\pi}\int_{-\infty}^{\infty} R_E(\tau)e^{i\omega\tau}d\tau \tag{2.24}$$

and is normalized via [40], to give

$$\langle|\vec{E}(\vec{R},t)|^2\rangle = R_E(0) = \int_{-\infty}^{\infty} S(\mathbf{q},\omega)d\omega. \tag{2.25}$$

It is now possible to use the function in Eqn 2.21 to express the correlation function $R_E(\tau)$ in terms of the correlation $\delta\varepsilon(\vec{r},t)$ and thus obtain a general expression for the spectral density [40],

$$S(\mathbf{q},\omega) = E_{0i}^2\Big(\frac{\omega_i}{c}\Big)^4\frac{\sin^2\phi}{(2\pi R)^2}(2\pi)^3\cdot\frac{1}{2\pi}\int_{-\infty}^{\infty} R_{\delta\varepsilon}(\tau)e^{i\omega_i\tau}e^{i\omega\tau}d\tau. \tag{2.26}$$

However there is now a new problem that arises from this result and that is finding an expression for the term $R_{\delta\varepsilon}$ where

$$R_{\delta\varepsilon} = \langle\delta\varepsilon(\mathbf{q},t+\tau)\delta\varepsilon^*(\mathbf{q},t)\rangle \tag{2.27}$$

is the correlation function for fluctuations in the dielectric constant ε. To find a solution to this problem we begin by considering two independent thermodynamic variables, pressure (P) and entropy (S), fluctuations in the dielectric constant can then be expressed as,

$$\delta\varepsilon = \Big(\frac{\partial\varepsilon}{\partial P}\Big)_S\cdot\delta P(\mathbf{q},t) + \Big(\frac{\partial\varepsilon}{\partial S}\Big)_P\cdot\delta S(\mathbf{q},t). \tag{2.28}$$

If now we assume the fluctuations in P and S are uncorrelated with respect to one another, then each term can be written separately. Considering only the first term

since this corresponds to adiabatic pressure fluctuations which are essentially sound waves then,

$$\delta\varepsilon = \Big(\frac{\partial\varepsilon}{\partial P}\Big)_S \cdot \delta P(\mathbf{q},t) \tag{2.29}$$

We note here that the term $\delta P(\mathbf{q},t)$ is the Fourier amplitude of the spatial component of pressure with a wavelength of $2\pi/\mathbf{q}$. We can assume that the sound wave travels with some angular frequency $\pm\omega_s(\mathbf{q})$ and has a lifetime of $1/\Gamma(\mathbf{q})$, in which case the correlation function of sound then becomes [40],

$$R_{\delta\varepsilon}(\tau)_{sound} = \Big(\frac{\partial\varepsilon}{\partial p}\Big)_S^2 \cdot \langle|\delta P(\mathbf{q},t)|^2\rangle e^{\pm i\omega t} e^{-\Gamma|\tau|} \tag{2.30}$$

It is now possible to rewrite the expression for spectral density for sound waves in Eqn 2.26 by substituting $R_{\delta\varepsilon}(\tau)_{sound}$ in Eqn 2.30 for $R_{\delta\varepsilon}(\tau)$ in Eqn. 2.27 and solving the integral to get [40]

$$\begin{aligned}\Big[S(\mathbf{q},\omega_s)\Big]_{sound} &= E_{0i}^2\Big(\frac{\omega_i}{c}\Big)^4 \frac{\sin^2\phi}{(2\pi R)^2}(2\pi)^3 \cdot \Big(\frac{\partial\varepsilon}{\partial p}\Big)_S^2 \cdot \langle|\delta P(\mathbf{q},t)|^2\rangle \\ &\frac{1}{\pi}\cdot\Big(\frac{\Gamma^2(\mathbf{q})}{\Gamma^2(\mathbf{q})+(\omega-(\omega_i-\omega_s))^2} + \frac{\Gamma^2(\mathbf{q})}{\Gamma^2(\mathbf{q})+(\omega-(\omega_i+\omega_s))^2}\Big)\end{aligned} \tag{2.31}$$

The last two terms in this expression represent Brillouin doublets which are centered at the frequencies, $\omega = \omega_i - \omega_s$ and $\omega = \omega_i + \omega_s$. The general line shape of this spectral function is a Lorentzian which is broadened by the factor $1/\Gamma(\mathbf{q})$. The full width at half maximum (FWHM) of this function is given by [41]

$$\Delta\omega_B = \Gamma(\mathbf{q}) = \frac{1}{2\rho}\left[\frac{4}{3}\eta_s + \eta_b + \frac{\kappa}{C_p}(\gamma-1)\right]\mathbf{q}^2. \tag{2.32}$$

where $eta_{s,b}$ is the shear and bulk viscosity, κ is the thermal conductivity of the liquid, ρ is the density of the liquid, and $\gamma = C_p/C_v$ is the ratio of specific heat at constant pressure C_p to the specific heat at constant volume C_v. The last term on the right is

neglected since $\gamma - 1 \simeq 0$ [29]. Taking this into consideration we can rewrite Eqn 2.32 as the following:

$$\Gamma(\mathbf{q}) = \frac{1}{2\rho}[\frac{4}{3}\eta_s + \eta_b]\mathbf{q^2} = \frac{1}{\rho}\eta_0\frac{2\pi^2 n^2}{\lambda_i^2} \tag{2.33}$$

where $\eta_0 = \frac{4}{3}\eta_s + \eta_b$ is the apparent viscosity and $\mathbf{q} = \dfrac{4\pi n}{\lambda_i}$ where n and λ_i are the refractive index and wavelength of incident light, respectively. If the shear viscosity, as well as other quantities (ρ, λ_i, and n) are known then the bulk viscosity of the fluid can be found from the FWHM of Brillouin peaks.

The result of the above derivation is a spectrum consisting of the intensity of the scattered light as a function of frequency where peaks are due to phonon modes. A typical spectrum for an isotropic liquid at room temperature is shown in Fig 2.4.

Brillouin spectroscopy is a useful technique for the study of molecular interactions in a fluid. The FWHM of Brillouin spectral peaks can yield important quantities of a fluid such as viscosity (as discussed previously) and also information on absorption of sound waves. Using the expression for FWHM $\Delta\omega_B$ in Eqn.2.32 along with the velocity of sound waves $v(\mathbf{q})$ obtained in Eqn. 2.11, then it is possible to calculate the frequency independent sound absorption α/f^2 given by [40],

$$\frac{\alpha}{f^2} = \frac{\pi\Delta\omega_B}{v(\mathbf{q})f^2} \tag{2.34}$$

The equations derived in this section are necessary for obtaining the results presented later in Chapter 4. The frequency shift obtained from Brillouin spectra will be used to calculate phonon velocities from Eqn. 2.11. As well, from the FWHM it is also possible to observe how the attenuation of sound waves varies as a function of temperature by using the relation in Eqn. 2.34.

2.3 Mechanical Properties of Fluids

The following discussion of mechanical properties of fluids, in particular, bulk modulus, follows the derivation previously presented in Ref. [40]. To begin consider a longitudinal wave propagating in an isotropic homogeneous medium where the particles in the medium oscillate in the direction of wave propagation. Consider the motion of an element (dx) of the medium which is small compared to the wavelength of sound and is initially contained between two plates, A and B with unit area, as seen in Figure 2.5.

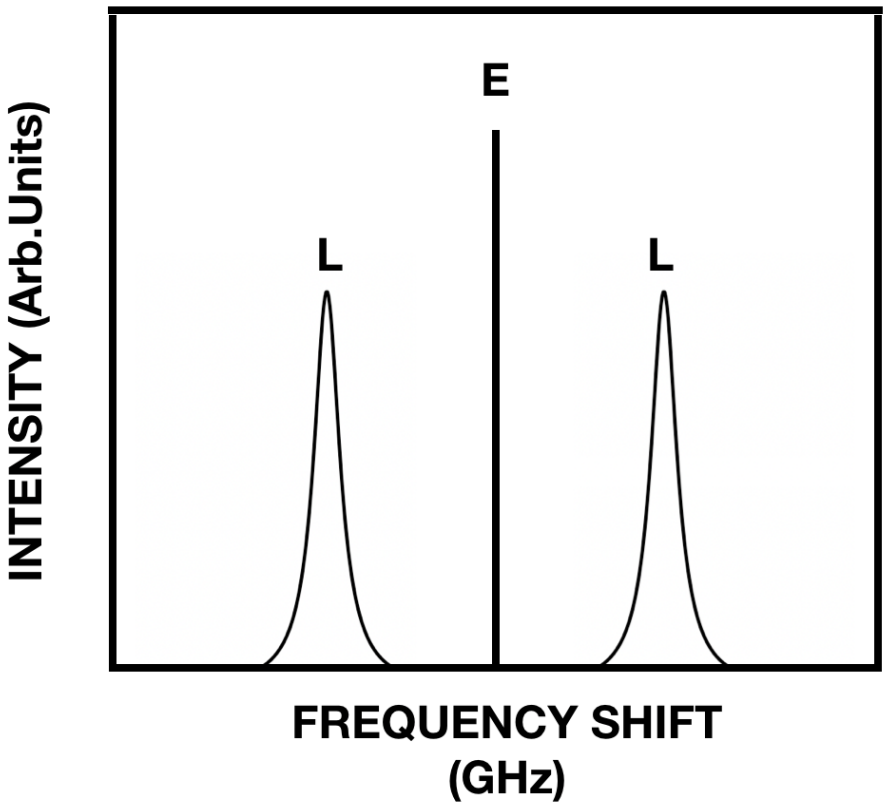

Figure 2.4: Schematic of a typical Brillouin spectrum for a liquid at room temperature. L indicates that these are longitudinal modes. E is the elastically scattering light via laser light.

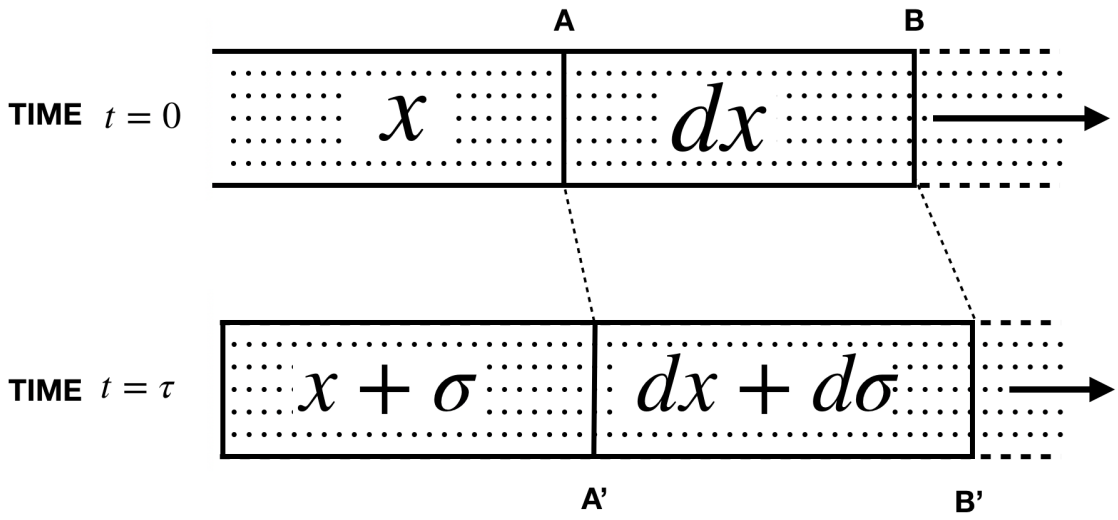

Figure 2.5: Schematic of wave propagation in an element of length dx in an isotropic medium between two plates **A** and **B** at time T = 0 (Top). (Bottom) After some time T = τ there is motion (depicted by arrow) in the medium, where element dx is now at positions **A′** and **B′** where the length of the element is now dx + dσ.

The plates are initially at distances x and $x + dx$ from an arbitrary reference point, and oriented perpendicular to the propagation direction. Let us begin by stating that ρ is the initial density of the medium with no sound waves present. In this case the mass of element dx is ρdx. After some time τ the element is now displaced to the position A' and B', where A' is the distance $x + \sigma$ from the origin and the length of the new element is $dx + d\sigma$. Utilizing the conservation of mass, the new density ρ' is given by [40],

$$\rho' = \rho \frac{dx}{dx + d\sigma} \tag{2.35}$$

The magnitude of the net force acting on the element is given by $F = PA$ where A is the area (in this case unit area) and $P = P_A - P_B$ is the hydrostatic pressure produced by the pressure of sound waves contained between plates A and B. Now setting this force equal to the product of mass of fluid contained in the volume element and its acceleration, one obtains

$$F = (P_{A'} - P_{B'})A = (\rho g h)A = (\frac{\partial P}{\partial x}dx)A \tag{2.36}$$

where the hydrostatic pressure $(P_{A'} - P_{B'})$ is equal to $\rho g h$ (Stevin's law) [42] and here the effects of gravity are neglected due to the small volume being considered [40]. Likewise, since we also have

$$F = \rho dx \frac{d^2\sigma}{dt^2} \tag{2.37}$$

where ρdx is the mass of element dx and $\dfrac{d^2\sigma}{dt^2}$ is acceleration since the plates have moved an additional distance σ with time t. Then equating Eqns. 2.36 and 2.37,

$$\rho \frac{d^2\sigma}{dt^2} = \frac{\partial P}{\partial x} = \frac{\partial P}{\partial \rho} \cdot \frac{\partial \rho}{\partial x} = \rho \frac{\partial P}{\partial \rho} \frac{d^2\sigma}{dx^2} \tag{2.38}$$

The equation of motion then becomes,

$$\frac{d^2\sigma}{dt^2} = \frac{\partial P}{\partial \rho} \frac{d^2\sigma}{dx^2} \tag{2.39}$$

From this result the factor $\dfrac{\partial P}{\partial \rho}$ has units of velocity squared [40], hence we can write

$$v^2 = \frac{\partial P}{\partial \rho} \tag{2.40}$$

Now assume that all the processes in a sound wave are reversible and adiabatic, then we can relate the velocity of the sound waves to the adiabatic bulk modulus [40],

$$B = -\frac{1}{V}\Big(\frac{\partial P}{\partial V}\Big)_S = \rho\Big(\frac{\partial P}{\partial \rho}\Big)_S. \tag{2.41}$$

Now we can rewrite Eqn 2.40 as

$$v^2 = \frac{\partial P}{\partial \rho} = \frac{B}{\rho}. \tag{2.42}$$

where v is the sound velocity, B is the bulk modulus, and ρ is the density of the material. In Brillouin scattering we can obtain the adiabatic bulk modulus from Eqn. 2.42 using the density ρ and velocity of sound waves from Eqn. 2.11.

Chapter 3

Experimental Setup

3.1 Sample Preparation

The gastropod mucus used in this work was bought commercially online at AliExpress and the precise composition of water and glycoproteins in this particular sample is unknown. The mucus was visually clear and looked like water to the eye, was quite viscous and was slimy to the touch. The mucus was kept in a sealed container at room temperature until a sample was extracted for use in experiments. The slug mucus was injected via syringe into a glass sample cell approximately 3/8" in diameter and about $\sim$ 15 cm long. The sample cell was sealed at one end by means of glassblowing and on the other end with a Teflon cap and epoxy. Due to expansion of the mucus during freezing, only approximately half of the glass cell was filled for experiments. After loading, the glass cell was placed in a sample holder as shown in Fig 3.2.

3.2 Variable Temperature Cell

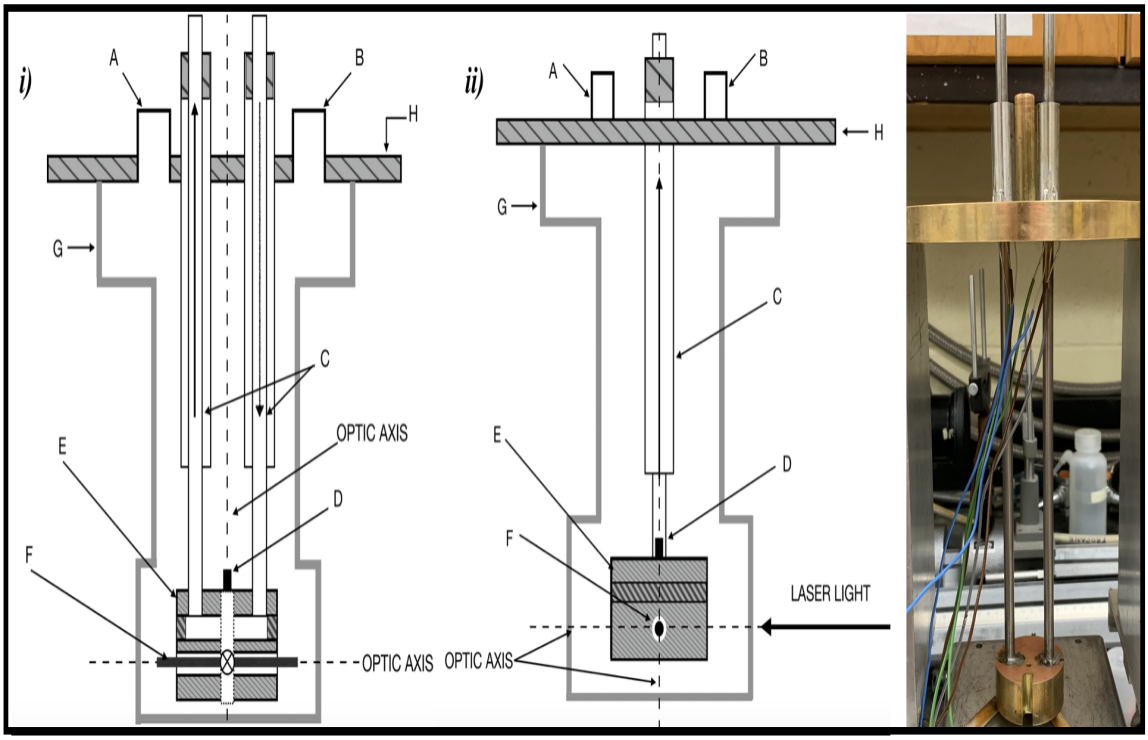

Figure 3.1: Schematic representation of variable temperature cell for front view i) and side view ii) used for heating and cooling samples. A - Electrical feed through, B - Vacuum feed through, C - Cooling Tubes, D - Silicon Diode, E - Brass Sample Holder, F - 50 Ω Resistor, G - Aluminum cell, H - Brass Plate. Image on the right is the actual apparatus used except for the aluminum cell.

A schematic representation of the variable temperature cell is shown in Fig 3.1. The sample holder was made from brass due to its extremely good thermal conductivity. The sample holder as shown in Fig 3.2 has two holes both 3/8" in diameter which can be used interchangeably for holding a sample in a glass vial and capable of holding a resistor. A thermal paste was added between the sample cell and sample holder such that there is good thermal contact between the glass sample cell and sample holder. It was necessary first to test the heating capability of multiple resistors to ensure the sample holder could heat up to the desired temperature. Resistors ranging

from 50 - 1000 Ω were tested and as a result of the heating tests, the 50 Ω resistor heated the quickest and was able to reach a temperature of 50 °C. An electrical feed-through was used for wiring the resistor and silicon diode. The resistor used is capable of achieving temperatures above 60 °C and was therefore suitable for this work. A roughing pump capable of achieving pressures of 10^{-3} Torr was used for evacuating the sample chamber to allow for proper temperature control of the sample holder. The cooling tubes allowed a fluid, in this case anti-freeze, to flow through the sample holder *E* in Figure 3.2. However, it was first necessary to test the cooling capabilities of the circulating bath from NESLAB Instruments. Tests were performed by allowing the antifreeze to flow through the cooling tubes and hence the sample holder in an attempt to achieve the lowest temperature. After 30-45 min, the temperature of the sample holder reached $\sim$ -22.0 °C. A second attempt, however, achieved only a temperature of $\sim$ -11.0 °C. The circulating bath was also capable of heating the sample holder via an internal heater in the circulating bath. This feature was used mainly to ensure temperature was maintained. A DT-670 series silicon diode from Lakeshore Cryotronics was used as a temperature sensor. The temperature, accurate to about $\pm$ 0.5 K, was obtained from the diode voltage using a standard calibration curve provided by Lakeshore Cryotronics.

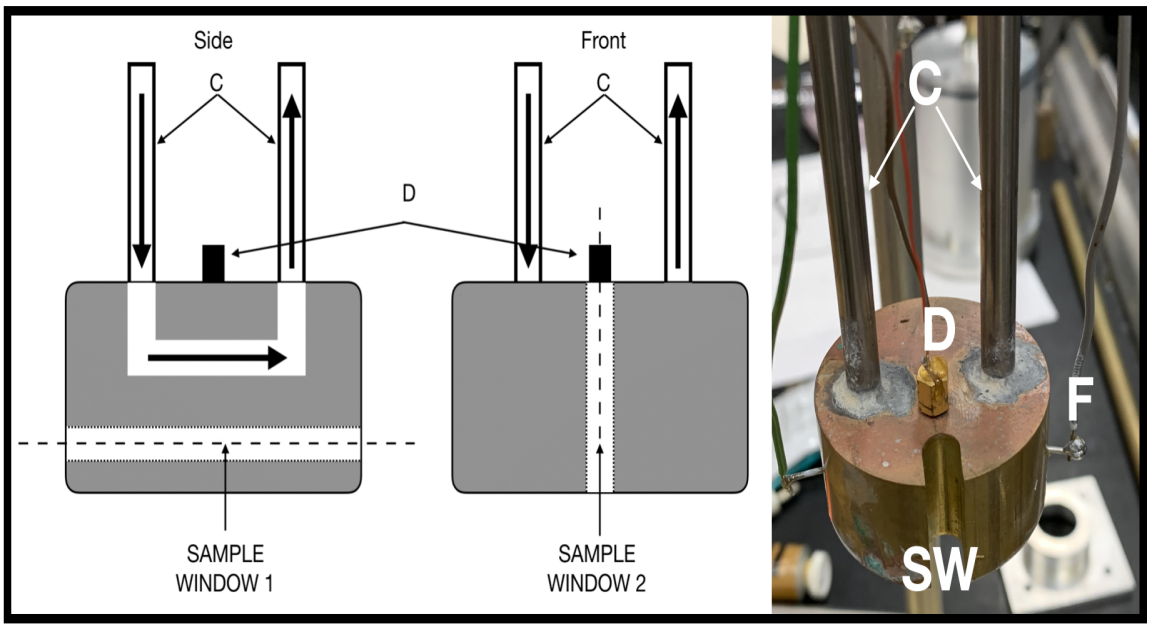

Figure 3.2: Schematic representation of brass sample holder used in the variable temperature cell. C - Cooling Tubes, D - Silicon Diode. Image on the right shows the actual brass holder used, F - Resistor, SW - Sample window.

A roughing pump and a temperature controller from Lakeshore Cryotronics which is shown in Fig 3.3 were also connected to the variable temperature cell. Operation of the temperature cell was fairly simple, however there were slightly different procedures for heating and cooling. First it was necessary to ensure that the temperature cell was fully evacuated. To do so the roughing pump was turned on for approximately 5 minutes. The roughing pump used was capable of evacuating the cell to about 10^{-2} to 10^{-3} Torr after just a few minutes. Next a voltage was set on the temperature controller (see Fig 3.3), corresponding to a temperature based on the standard curve provided by Lakeshore Cryotronics. The temperature of the sample holder, and hence the mucus, was monitored by a silicon diode as mentioned previously. If at first the sample was to be heated up, then after setting the voltage on the temperature controller, again corresponding to the desired temperature, then the 50 Ω resistor would begin heating the sample. To ensure the sample did not get too hot, the

circulating bath was turned on once the sample was close to the desired temperature. At this point it was crucial to adjust the knobs on the temperature controller (See Figure 3.3) to make sure the NULL meter reads 0. This was to assure that the heater (resistor) would turn off and the sample did not get too hot. If the sample holder started to cool below the desired temperature, the NULL meter would deviate from 0 and the heater would turn back on.

Figure 3.3: Image of temperature controller by Lakeshore Cryotronics used in this study.

The cooling process was similar to that for heating, except for the fact that initially the cooling control on the circulating bath was first turned on. Next the desired temperature on the circulating bath was selected using its dial. To ensure the sample did not get too cold, the temperature was set on the temperature controller and the heater was on if the sample holder got too cold. The circulating bath also had a built in heater so if the sample holder got colder than the desired temperature, the heater in circulating bath would turn on.

3.3 Brillouin Scattering Optical System

To collect Brillouin spectra of gastropod mucus, the optical setup shown in Figure 3.4 was used. The scattering geometry was a 180° backscattering with a Nd:YVO_4

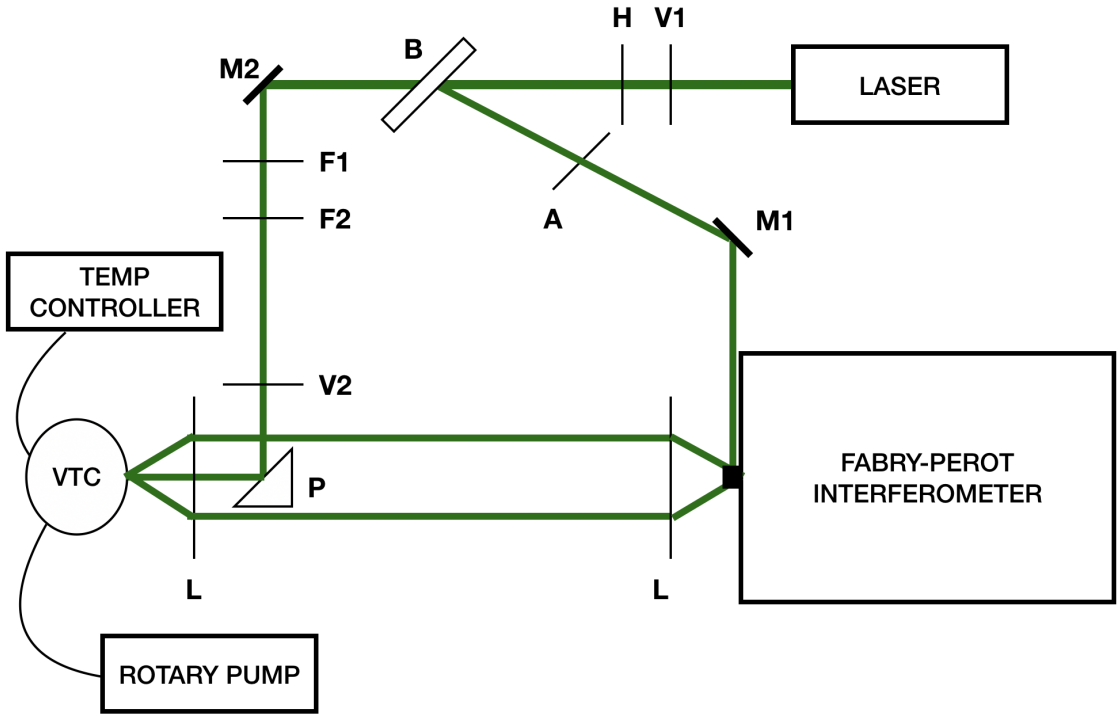

Figure 3.4: Optical setup for Brillouin scattering used in this study. $V_{1,2}$ - Variable neutral density filter, H - half wave plate, B - beam splitter, $M_{1,2}$ - mirror, $F_{1,2}$ - filter, VNDF - variable neutral density filter, A - aperture L- lens, P- prism, VTC - variable temperature cell.

solid state laser of wavelength 532 nm and output power of 2W as the incident light source.

The beam from the laser passes first through variable neutral density filter V_1 to reduce power and then passes through half-wave plate H to rotate the polarization of light from vertical to horizontal. Beam splitter B splits the beam such that part of the beam is reflected and the other part is transmitted. The portion that is reflected is used for aligning the Fabry-Perot Interferometer. This portion passes through an aperture A, then hits a mirror M_1, which redirects the beam through another variable neutral density filter V_2 where it then enters the Fabry Perot as a reference beam. The portion transmitted through the beam splitter hits a mirror M_2 which redirects the

beam through filters F_1 and F_2 to further reduce the beam power as it passes through another variable neutral density filter V_2 that reduces beam power to ≈ 100 mW. The beam then approaches a prism P where the beam is redirected and then focused on the sample inside the variable temperature cell (VTC) discussed previously by a camera lens L_C of focal length 5 cm. This camera lens was used to collect backscattered light from the sample and had an aperture of f/2.8. The scattered light from L_C is then focused on the input pinhole of the Fabry-Perot interferometer by lens L of focal length f = 40 cm. For this study the input pinhole was set to 450 μm.

The scattered light was analyzed by a six-pass tandem Fabry-Perot interferometer manufactured by JRS Scientific Instruments, a schematic of the apparatus can be seen in Fig 3.5 after Ref. [43]. This instrument is comprised of two Fabry-Perot interferometers labelled FP_1 and FP_2 with slightly different mirror spacings. The free spectral range used in this work was 30 GHz and the finesse was $\mathcal{F} \sim 100$.

After passing through the input pinhole, light is directed by mirrors M_1 and M_2 through aperture A_1 and is incident on FP_1. Only frequencies that satisfy

$$f_m = m\frac{c}{2nl\cos\theta} \tag{3.1}$$

are transmitted. Here m is any integer, n is the refractive index of the medium between the Fabry-Perot mirrors, and l is the mirror spacing and θ is the angle of incidence. Note that $n = 1$ in this work since the medium between the Fabry-Perot plates is air and $\theta = 0^\circ$ since the light is incident normally on the Fabry-Perot mirrors.

Equation 3.1 defines the resonance frequencies of the Fabry Perot [44] which then passes through aperture A_2.

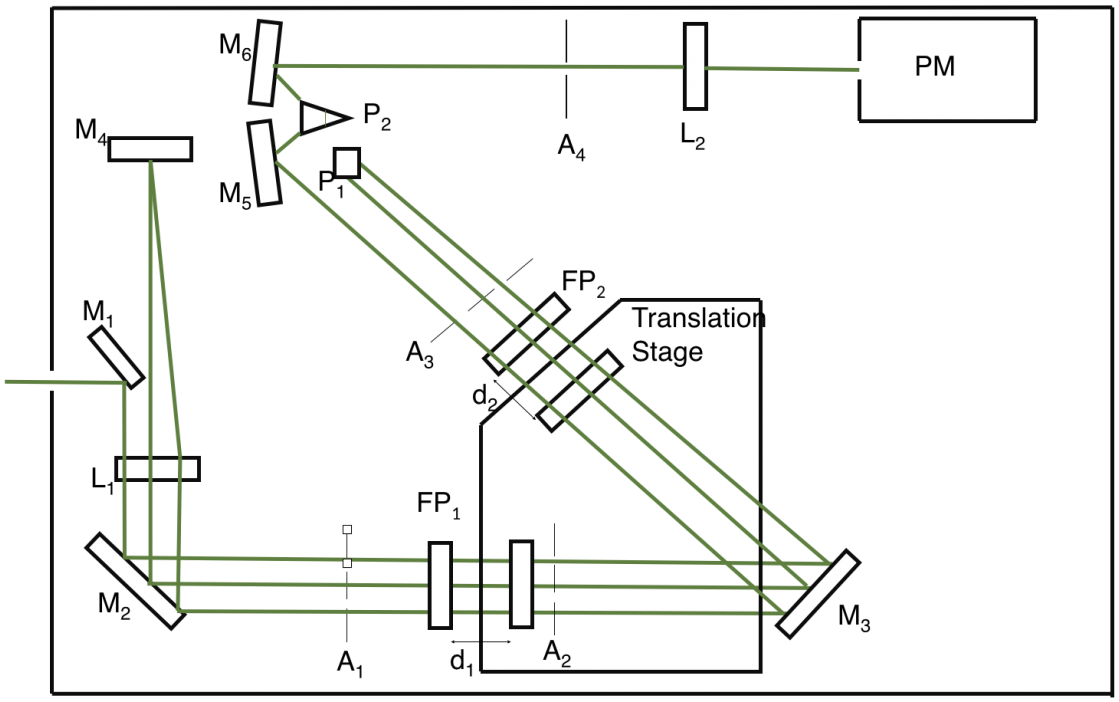

Figure 3.5: Schematic showing setup and optics of Fabry Perot interferometer. Mirror - $M_{1,2,3,4}$, Lens - $L_{1,2}$, Fabry Perot interferometer - $FP_{1,2}$, spacing of $FP_{1,2}$ - $d_{1,2}$, Prism - P , Photomultiplier - PM.

Light leaving aperture A_2 enters FP_2 after being redirected from mirror M_3. Since this is essentially the same Fabry-Perot as FP_1, only frequencies satisfying Equation 3.1 will again be transmitted. The beam is then incident on prism P_1 which redirects the beam back through aperture A_2. This beam passes through both Fabry Perot interferometers as well as through apertures A_1 and A_2 which is focused by lens L_1 onto mirror M_4. Mirror M_4 redirects the beam back through lens L_1 after which it completes another pass through the two interferometers, is incident on mirror M_6 and is detected by the photomultiplier tube PM. The photomultiplier tube sends information in electronic form to a computer which displays the frequency spectrum.

Chapter 4

Results and Discussion

4.1 Brillouin Spectra - General Features and Mode Assignment

Preliminary studies were initially collected on water and on mucus at room temperature as seen in Fig 4.1. It is evident that both the frequency shift between the two are very similar. Preliminary spectra yield frequency shifts of 7.3 GHz and 8.0 GHz for water and mucus, respectively. As well previous studies on water obtained a frequency shift for water of approximately 7.3 GHz which is very close to the frequency shift of mucus [45]. This is expected since mucus is composed mostly of water so one would expect the shifts to be relatively similar. Additionally, the sound velocity for the mucus mode has a magnitude on average of $\sim$ 1600 m/s which is very similar to that of water with a value of $\sim$ 1500 m/s. Figures 4.2 - 4.4 show the Brillouin spectra collected for samples of slug mucus studied over the temperature range -11°C $\leq$ T $\leq$ 52°C. Brillouin spectra were first collected from the highest temperature and all other spectra were collected as the temperature decreased. This being said, preliminary tests were conducted by collecting spectra as temperature was first lowered and then

as temperature was increased. No changes in the spectra at a given temperature were observed, indicating the absence of thermal hysteresis. A peak due to a longitudinal mode travelling in liquid mucus was observed for all temperatures at a shift of $\sim$ 8.0 GHz.

For temperatures T $\leq$ -2.5°C, a second peak at a frequency shift of $\sim$ 18.5 GHz was observed in the Brillouin spectra. Since this peak appears near the freezing point of water, this peak is attributed to ice forming in the mucus. As well the frequency shift of the 18.5 GHz peak and the frequency shift obtained for previous studies of ice I_h out at T = -3.0 °C [34], T = -16.0 °C [35] and T = -35.5°C [33] supports this assignment. The frequency shift for a longitudinal mode of ice was previously obtained using a 90° scattering geometry and a shift of 13.5 GHz was observed [34, 35]. Converting this to a frequency shift that would be obtained by a 180° scattering geometry (like that used in the present work) yields a frequency shift of $\sim$ 19.0 GHz. It is expected that the frequency shift of these modes will be similar but not identical due to the presence of the glycoproteins.

Using Eq 2.2, the sound velocity of the mode associated with the 18.5 GHz peak was found to be 3780 m/s at T = -2.5 °C which agrees with the value of $\sim$ 3800 m/s obtained for ice at T = -3.0 °C [34]. Likewise, the velocity of the mode corresponding to the 18.5 GHz peak is $\sim$ 3850 m/s at T = -11.0 °C which agrees with the value of 3850 m/s found for ice at T = -16.0 °C [35]. Moreover, the bulk modulus ($\sim \rho v^2$) obtained for ice I_h was found to be 8.89 GPa at T = -16.0 °C and 9.24 GPa at T = -35.5 °C [33, 35]. The bulk modulus obtained for the ice mode in the present study is $\sim$ 13.0 GPa and is independent of temperature over the range studied. The values obtained in the current study and previous studies are about the same magnitude. Again, it is expected that these values will be slightly different from those of pure ice due to the presence of glycoproteins. As well, since the linewidth of a peak due to

a sound wave in a liquid is directly proportional to viscosity, one would expect this peak to change with temperature if it were due to a liquid mode. However, since the FWHM remains constant, it suggests that this peak is due to a solid, in this case ice.

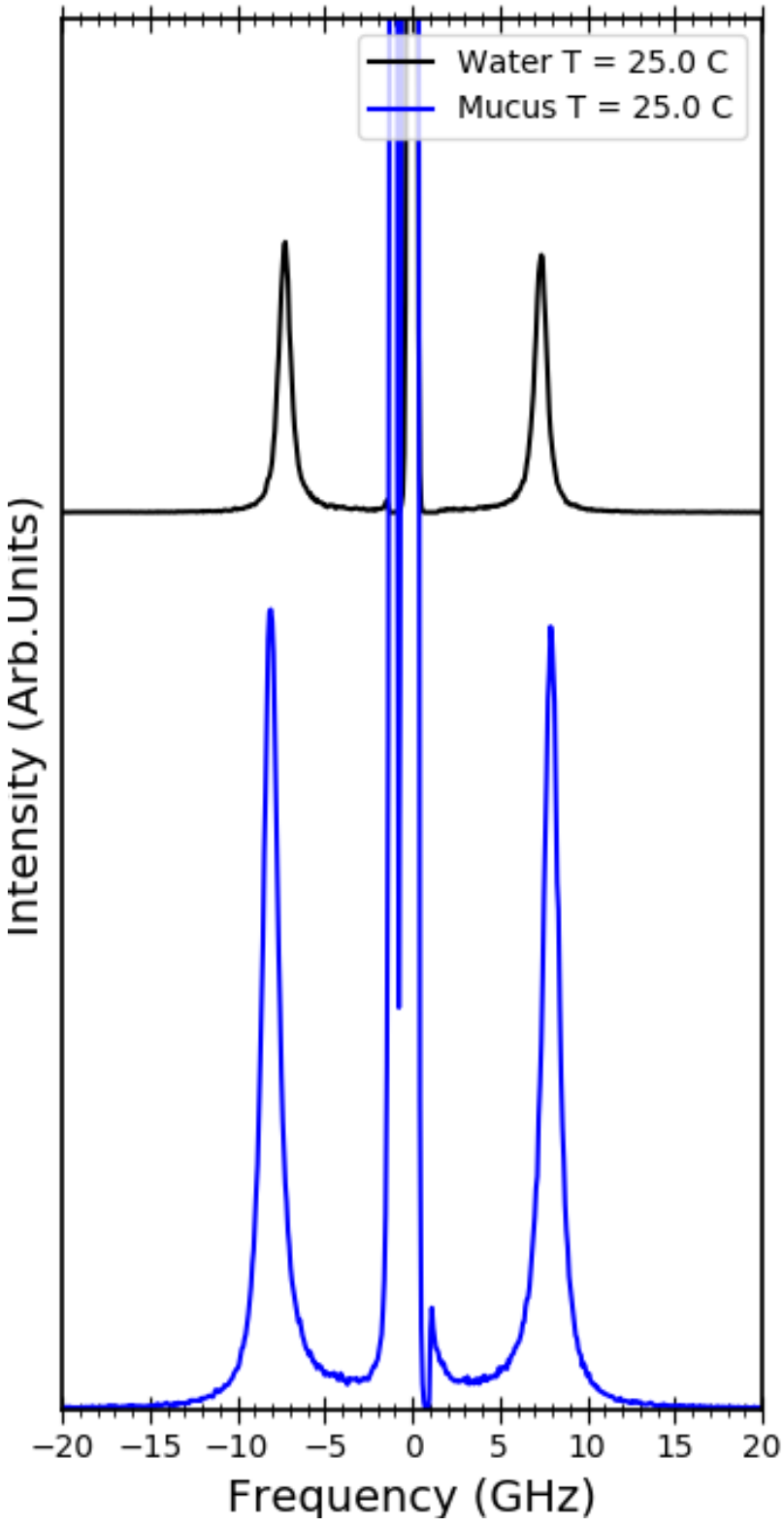

Figure 4.1: Preliminary Brillouin Spectra of water and gastropod mucus at room temperature.

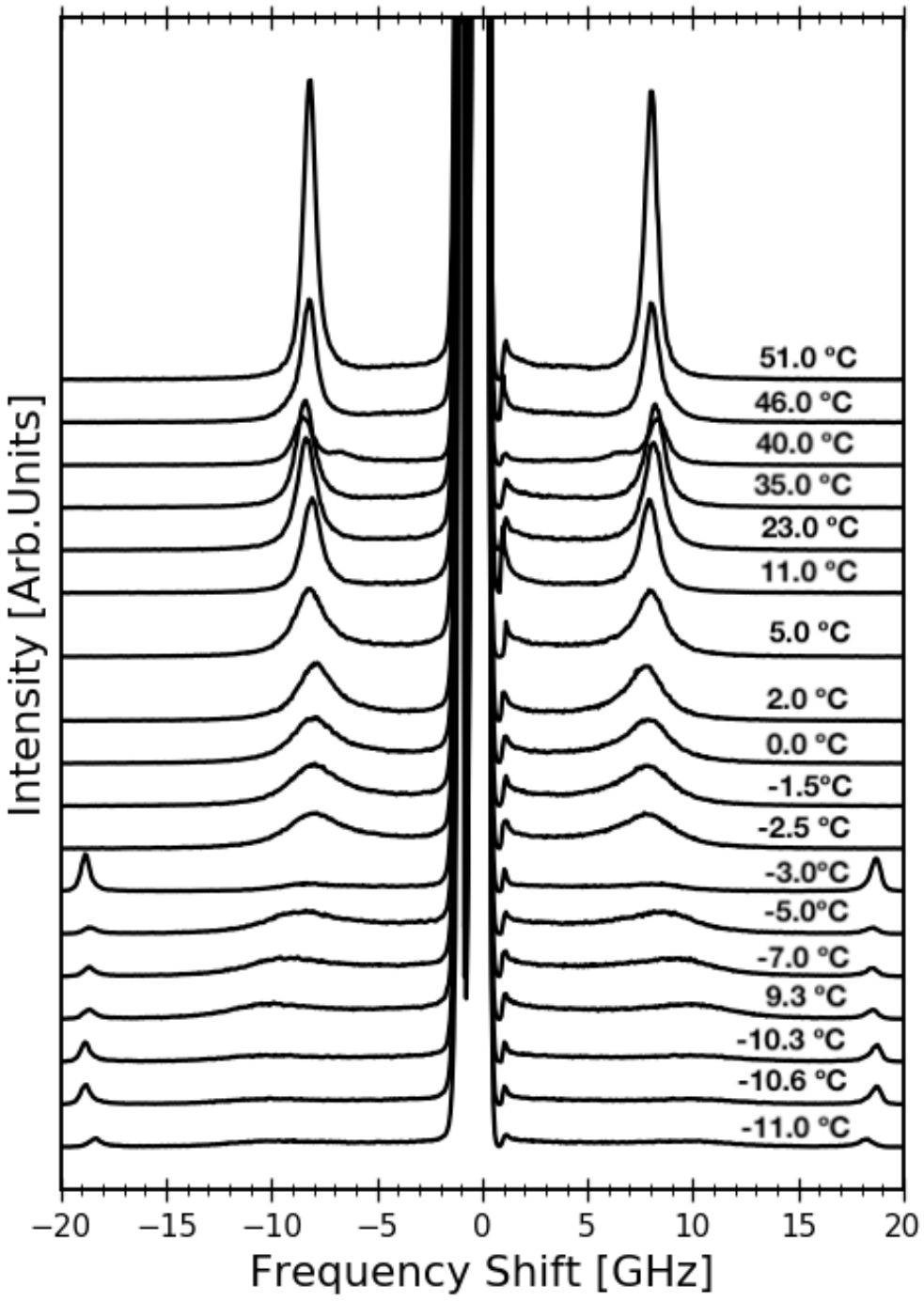

Figure 4.2: Brillouin spectra of gastropod mucus - Sample 1. Temperatures at which spectra were collected are indicated.

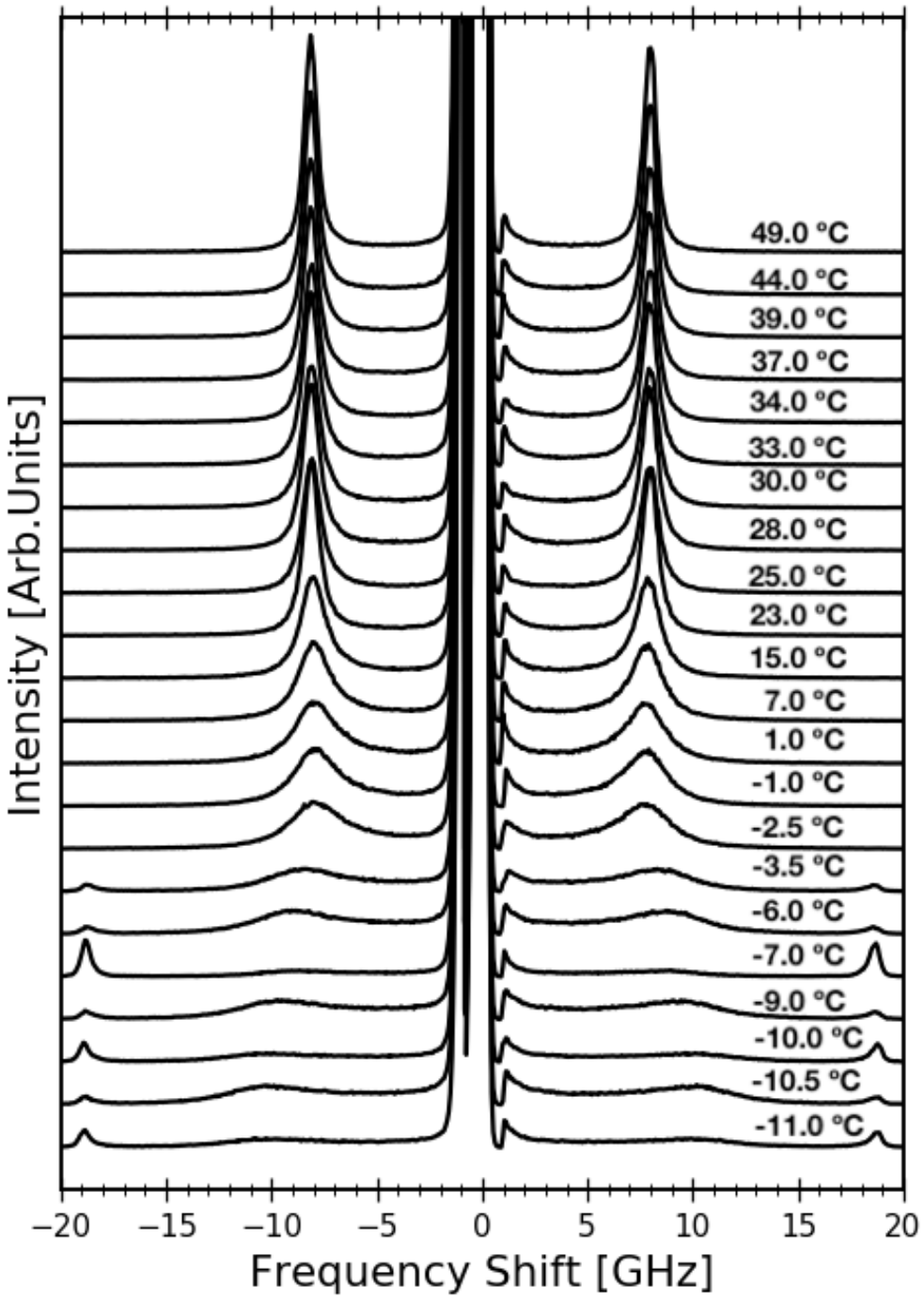

Figure 4.3: Brillouin Spectra of gastropod mucus - Sample 2. Temperatures at which spectra were collected are indicated.

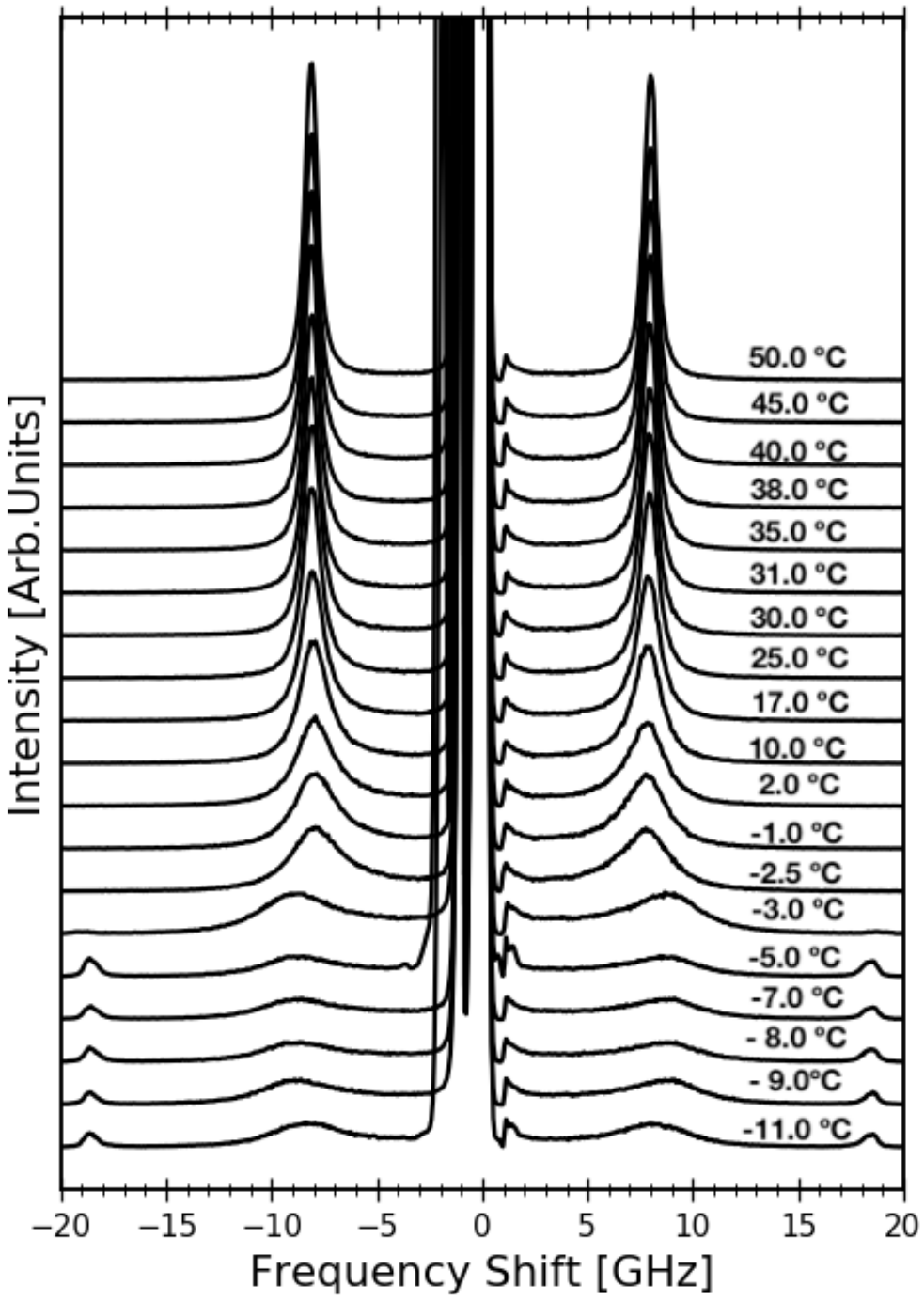

Figure 4.4: Brillouin Spectra of gastropod mucus - Sample 3. Temperatures at which spectra were collected are indicated.

Table 4.1: Brillouin frequency shift (f_M, f_I), FWHM$_M$, FWHM$_I$ and intensity (I_M,I_I) for spectral peaks in Sample 1, attributed to liquid (M) and solid (I) phases.

T [$\pm$ 0.5 K]	T [$\pm$ 0.5°C]	f_M [$\pm$ 0.3 GHz]	f_I [$\pm$ 0.1 GHz]	Δf_M [GHz]	Δf_I [$\pm$ 0.3 GHz]	I_M [Arb. Units]	I_I [Arb. Units]
324.0	51.0	8.1	—	0.7 ± 0.3	—	$13\,080 \pm 10$	—
319.0	46.0	8.1	—	0.8 ± 0.3	—	5800 ± 10	—
313.0	40.0	8.2	—	0.8 ± 0.3	—	$10\,374 \pm 10$	—
308.0	35.0	8.3	—	1.0 ± 0.3	—	6080 ± 10	—
296.0	23.0	8.2	—	1.0 ± 0.3	—	5220 ± 10	—
284.0	11.0	8.0	—	1.7 ± 0.3	—	5280 ± 10	—
278.0	5.0	7.8	—	2.2 ± 0.3	—	2090 ± 10	—
275.0	2.0	7.6	—	2.6 ± 0.3	—	2090 ± 10	—
273.0	0.0	7.7	—	2.7 ± 0.4	—	3200 ± 20	—
272.0	−1.5	7.4	—	3.5 ± 0.5	—	2110 ± 20	—
271.0	−2.5	7.6	18.5	4.1 ± 0.5	0.5	1700 ± 20	—
270.0	−3.0	7.7	18.6	4.8 ± 0.3	0.5	1410 ± 20	320 ± 20
268.0	−5.0	8.6	18.5	5 ± 1	0.5	1130 ± 20	460 ± 20
266.0	−7.0	8.8	18.8	6 ± 2	0.6	930 ± 20	870 ± 20
263.7	−9.3	9.1	18.8	9 ± 2	0.6	790 ± 20	900 ± 20
262.7	−10.3	9.0	18.8	10 ± 2	0.5	350 ± 20	1090 ± 10
262.4	−10.6	8.8	18.9	11 ± 3	0.5	230 ± 30	1620 ± 10
262.0	−11.0	8.1	18.7	13 ± 4	0.5	180 ± 30	1660 ± 10

Table 4.2: Brillouin frequency shift (f_M, f_I), FWHM$_M$, FWHM$_I$ and intensity (I_M,I_I) for spectral peaks in Sample 2, attributed to liquid (M) and solid (I) phases.

T [$\pm$ 0.5 K]	T [$\pm$ 0.5°C]	f_M [$\pm$ 0.3 GHz]	f_I [$\pm$ 0.1 GHz]	Δf_M [GHz]	Δf_I [$\pm$ 0.3 GHz]	I_M [Arb. Units]	I_I [Arb. Units]
322.0	49.0	8.1	—	0.6 ± 0.2	—	$10\,070 \pm 10$	—
317.0	44.0	8.1	—	0.7 ± 0.2	—	9350 ± 10	—
316.0	43.0	8.0	—	0.7 ± 0.2	—	8720 ± 10	—
312.0	39.0	8.0	—	0.8 ± 0.3	—	7990 ± 10	—
310.0	37.0	8.0	—	0.8 ± 0.2	—	8150 ± 10	—
307.0	34.0	8.0	—	0.8 ± 0.3	—	6770 ± 10	—
306.0	33.0	8.0	—	0.9 ± 0.3	—	8130 ± 10	—
303.0	30.0	8.0	—	1.0 ± 0.3	—	6830 ± 10	—
301.0	28.0	8.0	—	0.9 ± 0.3	—	7800 ± 10	—
298.0	25.0	8.0	—	1.0 ± 0.3	—	6500 ± 10	—
296.0	23.0	8.0	—	0.9 ± 0.3	—	8330 ± 20	—
288.0	15.0	7.9	—	1.4 ± 0.3	—	4770 ± 10	—
280.0	7.0	7.8	—	1.9 ± 0.3	—	3710 ± 20	—
274.0	1.0	7.7	—	2.6 ± 0.3	—	2910 ± 20	—
272.0	-1.0	7.7	—	2.9 ± 0.4	—	2710 ± 30	—
270.5	-2.5	7.6	—	3.6 ± 0.4	—	2220 ± 30	—
270.0	-3.0	7.9	18.6	5.8 ± 0.5	0.7	1080 ± 30	320 ± 10
267.0	-6.0	8.2	18.6	7.4 ± 0.5	0.7	1120 ± 30	350 ± 10
266.0	-7.0	8.6	18.7	9 ± 2	0.5	920 ± 30	370 ± 10
264.0	-9.0	8.4	18.7	10 ± 2	0.7	910 ± 40	380 ± 10
262.7	-10.3	8.6	18.8	11 ± 2	0.5	430 ± 40	890 ± 10
262.4	-10.6	8.6	18.7	12 ± 3	0.7	430 ± 40	750 ± 10
262.0	-11.0	8.4	18.8	13 ± 3	0.6	310 ± 40	1650 ± 10

Table 4.3: Brillouin frequency shift (f_M, f_I), FWHM$_M$, FWHM$_I$ and intensity (I_M,I_I) for spectral peaks in Sample 3, attributed to liquid (M) and solid (I) phases.

T [$\pm$ 0.5 K]	T [$\pm$ 0.5°C]	f_M [$\pm$ 0.3 GHz]	f_I [$\pm$ 0.1 GHz]	Δf_M [GHz]	Δf_I [$\pm$ 0.3 GHz]	I_M [Arb. Units]	I_I [Arb. Units]
323.0	50.0	8.1	—	0.7 ± 0.3	—	$14\,570 \pm 20$	—
318.0	45.0	8.0	—	0.7 ± 0.3	—	$13\,240 \pm 20$	—
313.0	40.0	8.0	—	0.8 ± 0.3	—	$12\,620 \pm 20$	—
311.0	38.0	8.0	—	0.8 ± 0.3	—	$12\,070 \pm 20$	—
308.0	35.0	8.0	—	0.9 ± 0.6	—	$10\,860 \pm 20$	—
304.0	31.0	8.0	—	0.9 ± 0.5	—	9860 ± 20	—
303.0	30.0	8.0	—	1.0 ± 0.5	—	9660 ± 20	—
299.0	26.0	8.0	—	1.0 ± 0.4	—	8820 ± 20	—
290.0	17.0	7.9	—	1.3 ± 0.5	—	6910 ± 20	—
283.0	10.0	7.9	—	1.6 ± 0.5	—	5630 ± 30	—
275.0	2.0	7.8	—	2.2 ± 0.6	—	4080 ± 30	—
272.0	−1.0	7.8	—	2.6 ± 0.5	—	3530 ± 30	—
271.0	−2.5	7.7	—	3.2 ± 0.6	—	3000 ± 20	—
270.0	−3.0	8.0	18.5	5 ± 1	0.7	1150 ± 30	290 ± 10
268.0	−5.0	8.2	18.5	6 ± 2	0.7	970 ± 30	810 ± 10
266.0	−7.0	8.3	18.5	8 ± 2	0.7	990 ± 30	600 ± 10
265.0	−8.0	8.4	18.5	9 ± 2	0.7	930 ± 30	650 ± 10
264.0	−9.0	8.4	18.6	11 ± 3	0.6	1190 ± 30	590 ± 10
262.0	−11.0	8.5	18.8	12 ± 4	0.8	1940 ± 30	840 ± 10

4.2 Sound Velocity - Temperature Dependence

Tables 4.1 - 4.3 show the frequency shifts of both mucus and ice peaks observed for samples studied in this work. The frequency shifts were obtained by fitting a Lorentzian function to the Stokes and anti-Stokes peaks and taking the average between these values. Uncertainty in the frequency shift came from the uncertainty in the Lorentzian fit. The fitting algorithm can be found in Appendix A.

Figures 4.5 - 4.7 show the frequency shift as a function of temperature for the mucus and ice peaks. As shown in these figures, the frequency shift for the mucus peak decreases slightly from $\sim$ 8.1 GHz at T = 50.0 °C to $\sim$ 7.6 GHz at T = -2.5°C. Below T = -2.5°C there is a rapid increase in the frequency shift of the mucus peak from 7.7 GHz at T = -2.5°C to $\sim$ 8.8 GHz at T = -11.0°C. In contrast, the shift of the peak due to ice remains relatively constant over the full temperature range with values slightly increasing from $\sim$ 18.5 GHz at T = -2.5 °C to $\sim$ 18.7 at T = -11.0°C.

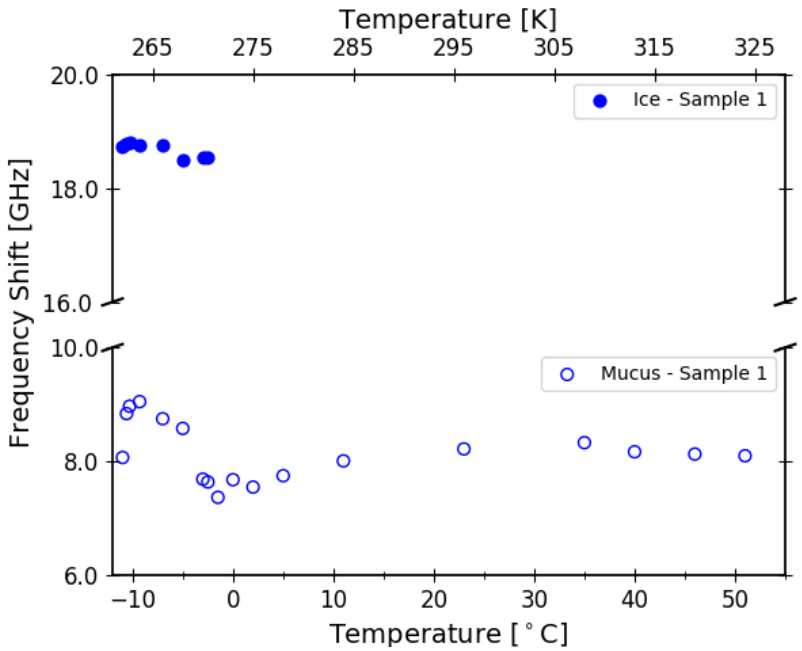

Figure 4.5: Frequency shift as a function of temperature for gastropod mucus - Sample 1. ○ - Mucus mode, ● - Ice mode.

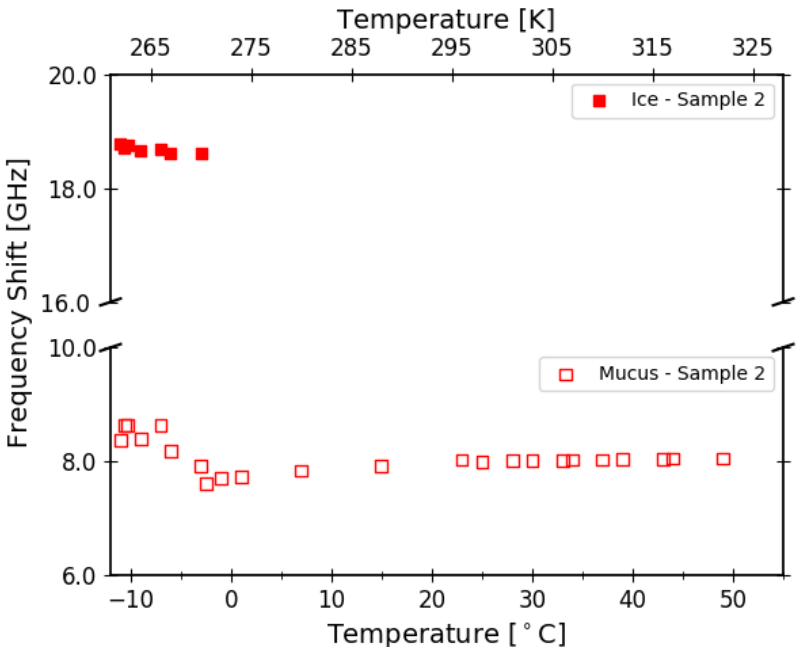

Figure 4.6: Frequency shift as a function of temperature for gastropod mucus - Sample 2. □ - Mucus mode, ■ - Ice mode.

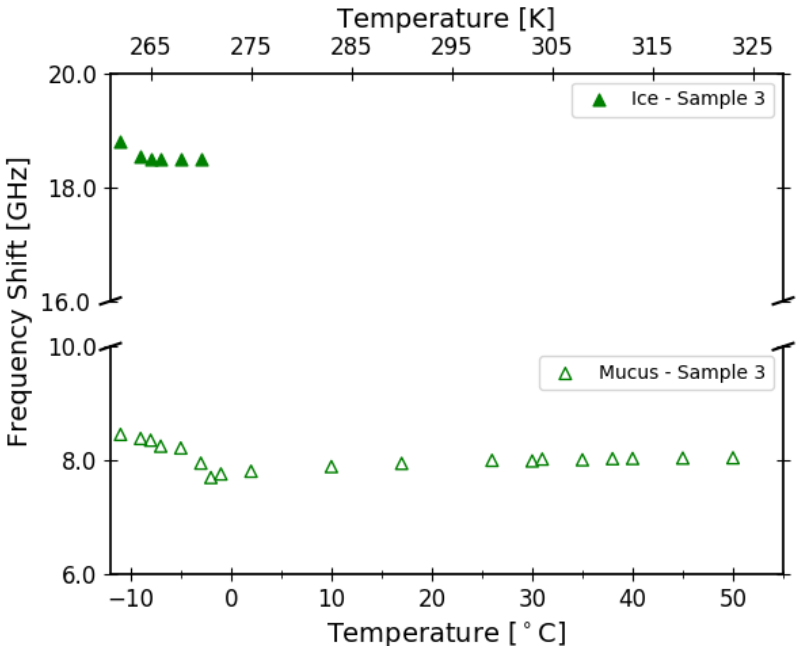

Figure 4.7: Frequency shift as a function of temperature for gastropod mucus - Sample 3. △ - Mucus mode, ▲ - Ice mode.

Phonon velocities for snail mucus were calculated from Equation 2.2 using the frequency shifts in Table 4.1 - 4.3 and an average refractive index of water of $n = 1.33 \pm 0.01$ [46]. The resulting phonon velocities are tabulated in Tables 4.4. Uncertainty in acoustic velocities were calculated using standard error analysis formulae based on uncertainties in both frequency shifts (as shown in Table 4.1 - 4.3) and the refractive index n.

The sound velocity as a function of temperature is shown in Figures 4.8 - 4.10. The sound velocity of the mucus mode increases slightly for temperatures above T = -2.5°C with a value of $\sim$ 1580 m/s at T = -2.5°C to $\sim$ 1660 m/s at T = 50.0°C. Below T = -2.5°C there is a rapid increase in sound velocity for the mucus mode, with values increasing from $\sim$ 1580 m/s at T = -2.5°C to $\sim$ 1730 m/s at -11.0°C. The ice mode shows a slight increase from its value of 3770 m/s at T = -2.5°C to 3840 m/s at T = -11.0°C. The sound velocities obtained for both the mucus and ice mode show consistency in the values between each sample.

Table 4.4: Phonon velocities (v_M, v_I) calculated for all samples using Equation 2.2, attributed to liquid (M) and solid (I) phase.

Sample 1				Sample 2				Sample 3			
T [± 0.5 K]	T [±0.5°C]	v_M [± 60 m/s]	v_I [± 20 m/s]	T [± 0.5 K]	T [±0.5°C]	v_M [± 60 m/s]	v_I [± 20 m/s]	T [± 0.5 K]	T [±0.5°C]	v_M [± 60 m/s]	v_I [± 20 m/s]
324.0	51.0	1660	—	322.0	49.0	1640	—	323.0	50.0	1650	—
319.0	46.0	1670	—	317.0	44.0	1640	—	318.0	45.0	1650	—
313.0	40.0	1670	—	316.0	43.0	1640	—	313.0	40.0	1640	—
308.0	35.0	1700	—	312.0	39.0	1650	—	311.0	38.0	1640	—
296.0	23.0	1680	—	310.0	37.0	1650	—	308.0	35.0	1640	—
284.0	11.0	1640	—	307.0	34.0	1650	—	304.0	31.0	1640	—
278.0	5.0	1550	—	306.0	33.0	1650	—	303.0	30.0	1640	—
275.0	2.0	1580	—	303.0	30.0	1640	—	298.0	25.0	1640	—
273.0	0.0	1570	—	301.0	28.0	1640	—	290.0	17.0	1630	—
272.0	−1.5	1510	—	298.0	25.0	1640	—	283.0	10.0	1610	—
271.0	−2.5	1570	3770	296.0	23.0	1640	—	275.0	2.0	1600	—
270.0	−3.0	1570	3800	288.0	15.0	1620	—	272.0	−1.0	1590	—
268.0	−5.0	1670	3810	280.0	7.0	1600	—	271.0	−2.5	1580	—
266.0	−7.0	1750	3840	274.0	1.0	1580	—	270.0	−3.0	1630	3780
264.0	−9.3	1850	3840	272.0	−1.0	1580	—	268.0	−5.0	1680	3780
263.0	−10.3	1830	3850	271.0	−2.5	1560	—	266.0	−7.0	1700	3780
262.0	−10.6	1810	3840	270.0	−3.0	1620	3810	265.0	−8.0	1710	3780
262.0	−11.0	1650	3840	267.0	−6.0	1680	3805	264.0	−9.0	1720	3790
				266.0	−7.0	1770	3830	262.0	−11.0	1730	3850
				264.0	−9.3	1720	3820				
				263.0	−10.3	1770	3830				
				262.0	−10.6	1770	3830				
				262.0	−11.0	1710	3840				

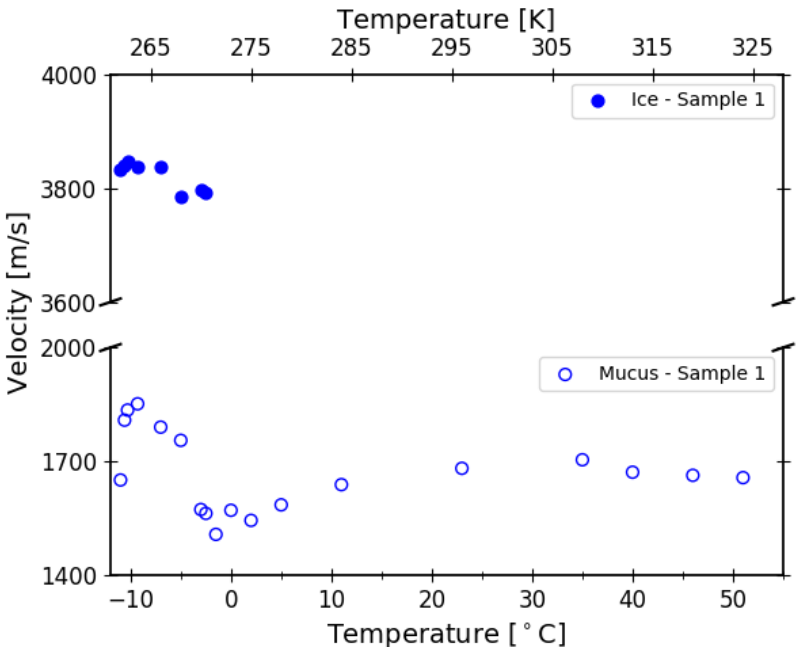

Figure 4.8: Sound wave velocity versus temperature for gastropod mucus - Sample 1. ○ - Mucus mode, ● - Ice mode.

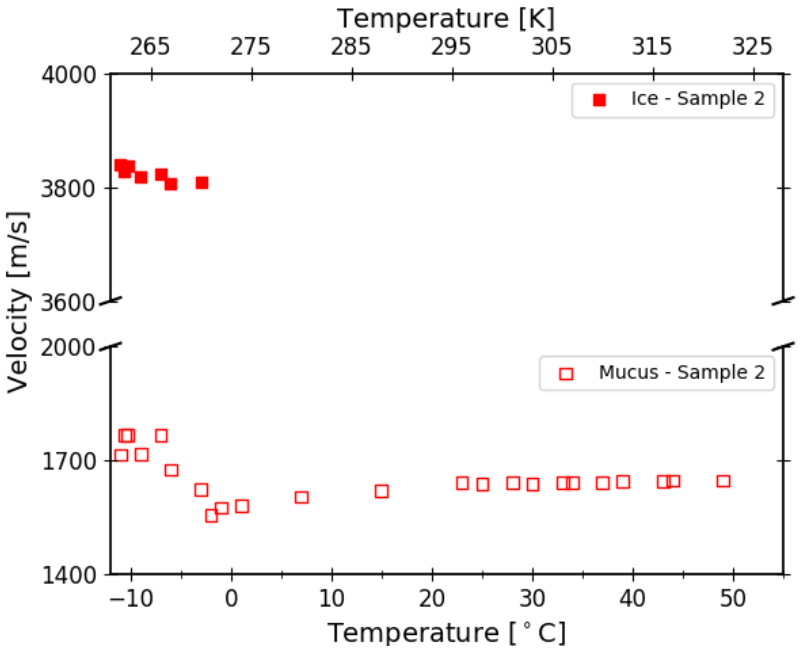

Figure 4.9: Sound wave velocity versus temperature for gastropod mucus - Sample 2. □ - Mucus mode, ■ - Ice mode.

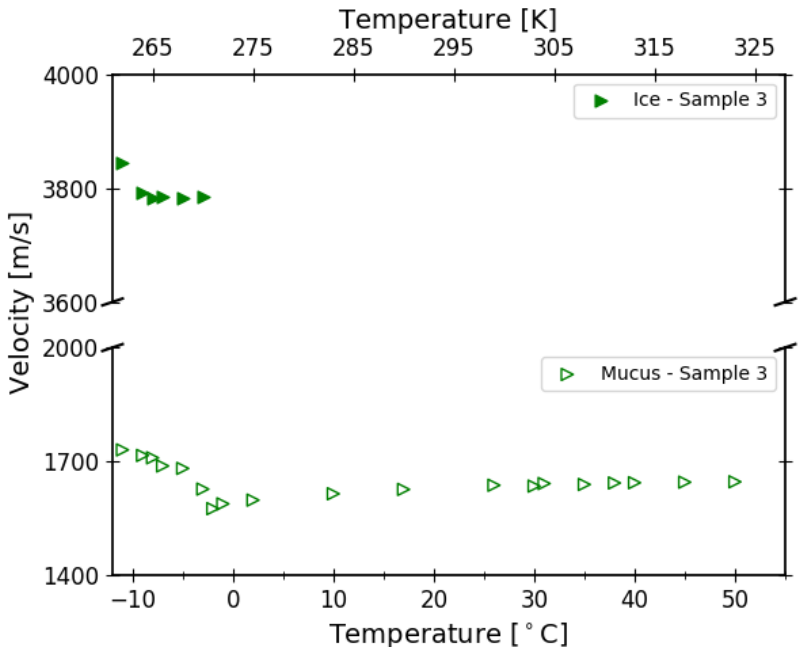

Figure 4.10: Sound wave velocity versus temperature for gastropod mucus - Sample 1. △ - Mucus mode, ▲ - Ice mode.

Since the work done in this project is original, direct comparison to other Brillouin scattering studies on gastropod mucus cannot be made. However, since the primary component of the mucus is water, the acoustic velocity of gastropod mucus and water will be compared [29–31]. As well, comparisons to related liquids such as mixtures of ethanol-water [27], polyvinylpyrrolidone-water [28] and polyethylene-water [47] will also be discussed. Likewise, comparison between previous studies on the sound velocity of ice I_h will be made with the values obtained in this study.

The sound velocity of the mucus mode found in the present work show similarities to the values of sound velocity obtained for water at temperatures greater than T = 0°C. The sound velocity of water at T = 0°C and 50°C was found to be 1350 m/s and 1550 m/s, respectively [29]. However the present study finds the sound velocities for the mucus mode at T = 0°C and 50°C to be 1600 m/s and 1650 m/s, respectively. The sound velocity of water increases at $\sim$ 4 m/s/°C which is four times the rate

at which sound velocity increases for the mucus mode over the temperature range 0 °C $\leq$ T $\leq$ 50 °C [29–31]. For temperatures below T = 0°C, it was observed that sound velocity for water decreases rapidly from $\sim$ 1400 m/s at T = 0°C to 1290 m/s at T = -10.0 °. This behaviour was not seen in the sound velocity for the mucus mode. In fact, for temperatures below -2.5°C, there is a sudden and steep increase in sound velocity with a difference of about 13% between values at T = -2.5°C and T = -11.0°C respectively. Furthermore, the rate at which the velocity of the water mode decreases below 0°C is about $\sim$ 8.0 m/s/°C, whereas the sound velocity of the mucus mode increases at a rate of $\sim$ 15 m/s/°C below T = -2.5°C. Likewise with regard to sound velocities measured at T = -10°C, a value of $\sim$ 1300 m/s was observed for supercooled water. This differs by about $\sim$ 30% from the sound velocity of 1780 m/s at obtained at T = -10 °C for the mucus mode [29, 30]. The cause for such difference in sound velocity between the mucus and water mode for temperatures T $\leq$ 0°C is likely due to the fact that supercooled water remains in a liquid state below 0 °C whereas snail mucus has ice crystals present below T = -2.5°C. As mentioned previously, the presence of ice in the mucus below T = -2.5°C influences the elastic properties of the liquid mucus in this temperature regime. The likely cause of this is due to the fact that as the temperature decreases, the water turns to ice leaving a higher concentration of glycoproteins in the mucus.

Solutions of liquids that have some similarities to that of the snail mucus (water and glycoproteins), such as mixtures of ethanol-water (EW) [47], polyvinyl pyrrolidone-water (PPW) and polyethylene glycol-water (PEGW) [27] record sound velocities for temperatures that fall in the same range as those studied in this work. Ultrasonic sound velocity was measured for varying concentrations of ethanol in ethanol-water solutions as a function of temperature [47]. Ethanol and water is similar to mucus in the sense that it is a compound mixed with water. For low concentrations of ethanol,

the sound velocity of EW increased with increasing temperature. Considering concentrations of 3 - 7 % ethanol by weight, the sound velocity increases at rates, 1 m/s/°C at 3 % ethanol and -1 m/s/°C at 7 % ethanol between 0 °C $\leq$ T $\leq$ 50 °C. As mentioned in Chapter 1, the concentration of glycoproteins in mucus is $\sim$ 3 - 7%, the sound velocity obtained over this temperature range also increases at a rate of 1 m/s/°C which is exactly like the ethanol and water mixture. The velocity of an ethanol-water mixture with an ethanol concentration of $\sim$ 3 % at T = 0°C and T = 50°C were found to be $\sim$ 1500 m/s and 1550 m/s, respectively. These velocities are approximately the same as the velocities found for the mucus mode at these temperatures. Similarly, the sound velocity was obtained for different concentrations of polyethylene glycol and water mixtures (PEGW) [27]. For a concentration 5% polyethylene glycol and 95% water by weight, the sound velocity of PEGW increased slightly over the range 300K $\leq$ T $\leq$ 360K at a rate of $\sim$ 0.5 m/s/K. Similarly, for concentrations of 5% polyvinylpyrrolidone and 95% water, the velocity increased from 1508 m/s at T = 0 °C to 1555 m/s at T = 45 °C. This is an increase of about $\sim$ 1.7 m/s/°C which is slightly higher than the increase of 1.0 m/s/°C obtained for snail mucus in this work over the range 0 °C $\leq$ T $\leq$ 50 °C.

4.3 Bulk Modulus - Temperature Dependence

The bulk moduli of both the liquid mucus and ice as a function of temperature were calculated using Eqn 2.42 which relies on the density and sound velocity, the results are tabulated in Table 4.5. The density of mucus was taken to be 1040 $\pm$ 30 kg/m^3 and was obtained by measuring the mass of a small portion of mucus ($\sim$ 100ml) and dividing by the volume. For ice, a density of 917.5 kg/m^3 was used [34]. Uncertainty in the bulk modulus was calculated using standard error analysis formulae with the

uncertainty in velocity from Table 4.4 as well as the uncertainty in density.

Figures 4.11 - 4.13 shows the bulk modulus as a function of temperature. The values of bulk modulus for the liquid mucus shows a slight increase from $\sim$ 2.7 GPa at T = -2.5°C to $\sim$ 3.0 GPa at T = 50.0°C. Below T = -2.5°C, the bulk modulus of the mucus increases with decreasing temperature at a rate of $\sim$ 0.2 GPa/°C with a maximum value of 4.0 GPa occurring at T = -11.0 °C. Similarly, the ice mode shows a slight increase in bulk modulus as temperature decreases with values increasing from $\sim$ 13.0 GPa at T = -2.5°C to $\sim$ 13.5 GPa at T = -11.0°C.

Table 4.5: Bulk modulus calculated using Equation 2.42 for both mucus and ice at different temperatures for all samples.

Sample 1				Sample 2				Sample 3			
T [± 0.5] [K]	T [±0.5] [°C]	B_M [± 0.5] [GPa]	B_I [± 0.9] [GPa]	T [± 0.5] [K]	T [±0.5] [°C]	B_M [± 0.5] [GPa]	B_I [± 0.9] [GPa]	T [± 0.5] [K]	T [±0.5] [°C]	B_M [± 0.5] [GPa]	B_I [± 0.9] [GPa]
324.0	51.0	3.0	—	322.0	49.0	3.0	—	323.0	50.0	3.0	—
319.0	46.0	3.0	—	317.0	44.0	3.0	—	318.0	45.0	3.0	—
313.0	40.0	3.1	—	316.0	43.0	3.0	—	313.0	40.0	3.0	—
308.0	35.0	3.2	—	312.0	39.0	3.0	—	311.0	38.0	3.0	—
296.0	23.0	3.1	—	310.0	37.0	3.0	—	308.0	35.0	3.0	—
284.0	11.0	3.0	—	307.0	34.0	3.0	—	304.0	31.0	3.0	—
278.0	5.0	2.8	—	306.0	33.0	3.0	—	303.0	30.0	2.9	—
275.0	2.0	2.6	—	303.0	30.0	3.0	—	298.0	25.0	2.9	—
273.0	0.0	2.7	—	301.0	28.0	3.0	—	290.0	17.0	2.9	—
272.0	−1.5	2.5	—	298.0	25.0	2.9	—	283.0	10.0	2.9	—
271.0	−2.5	2.7	13.2	296.0	23.0	3.0	—	275.0	2.0	2.8	—
270.0	−3.0	2.7	13.2	288.0	15.0	2.9	—	272.0	−1.0	2.8	—
268.0	−5.0	3.4	13.1	280.0	7.0	2.8	—	271.0	−2.5	2.7	—
266.0	−7.0	3.5	13.5	274.0	1.0	2.6	—	270.0	−3.0	2.9	13.1
264.0	−9.3	3.8	13.5	272.0	−1.0	2.7	—	268.0	−5.0	3.1	13.1
263.0	−10.3	3.7	13.6	271.0	−2.5	2.7	—	266.0	−7.0	3.1	13.1
262.0	−10.6	3.6	13.5	270.0	−3.0	2.9	13.3	265.0	−8.0	3.2	13.1
262.0	−11.0	4.0	13.5	267.0	−6.0	3.1	13.3	264.0	−9.0	3.2	13.2
				266.0	−7.0	3.2	13.4		−11.0	3.3	13.5
				264.0	−9.0	3.2	13.4				
				263.0	−10.3	3.4	13.5				
				262.0	−10.6	3.4	13.4				
				262.0	−11.0	3.2	13.5				

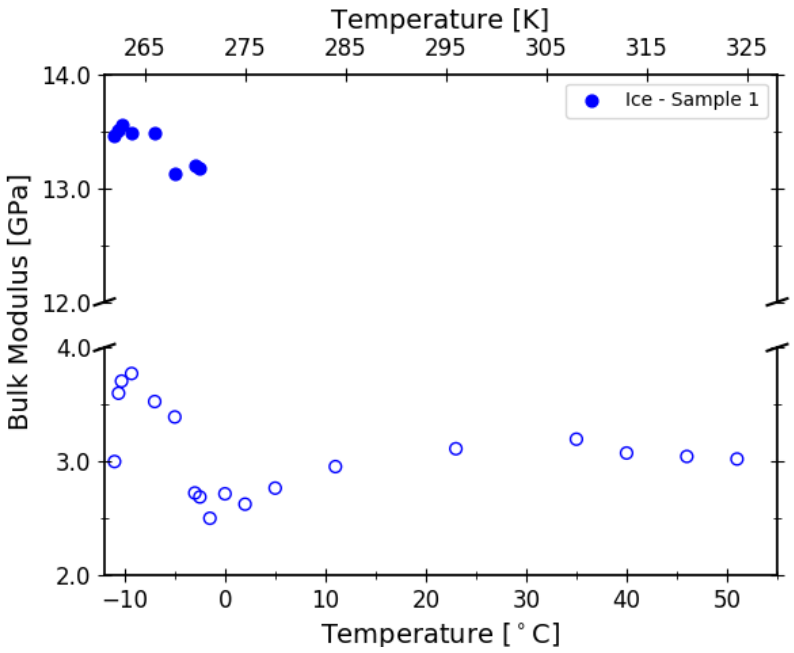

Figure 4.11: Bulk Modulus for gastropod mucus - Sample 1 as a function of temperature. ○ - Mucus, ● - Ice.

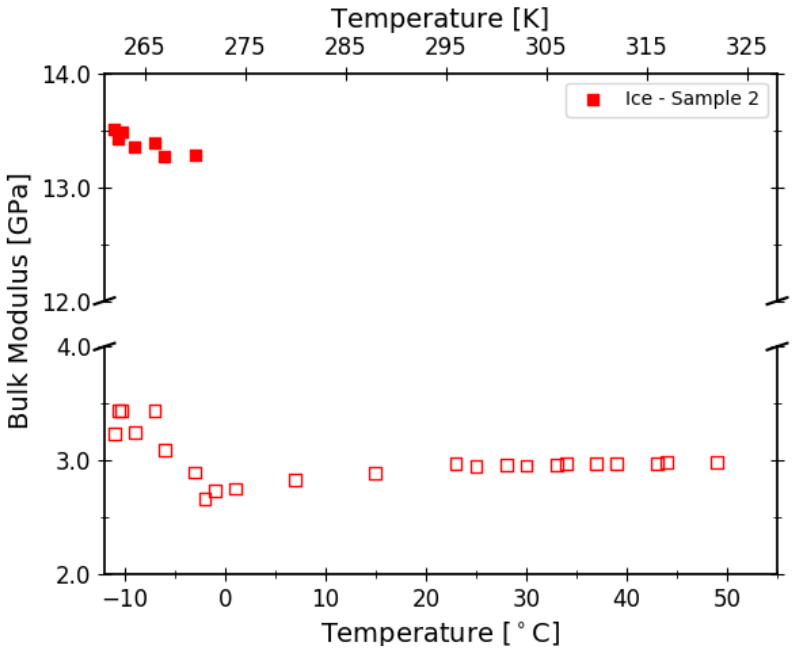

Figure 4.12: Bulk Modulus for gastropod mucus - Sample 2 as a function of temperature. □ - Mucus, ■ - Ice.

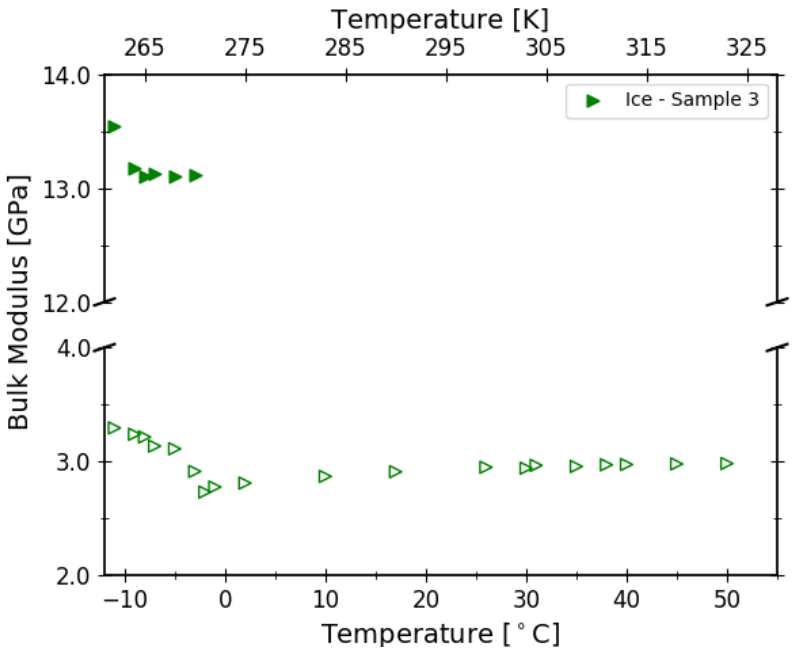

Figure 4.13: Bulk Modulus for gastropod mucus - Sample 2 as a function of temperature. ▷ - Mucus, ▶ - Ice.

Brillouin scattering was used previously to investigate the elastic properties of ice I_h at a temperature of -35.5°C [33]. In this study the bulk modulus of ice was reported to have a value of 9.24 GPa which differs by about 33% from the value reported in the present work which is $\sim$ 13.0 GPa at a temperature of -3 °C. It is important to note however that these two values were obtained at T = - 35.5 °C and -11.0°C for the work in Ref. [33] and are expected to be comparable but not exactly the same as the results obtained in the present work. The bulk modulus was also obtained for polycrystalline ice by Brillouin scattering at T = -16°C and a value of approximately 8.89 GPa was recorded [35]. This value is consistent with the previously obtained bulk modulus of ice at -35.5°C but differs from the current work by $\sim$ 38%. Based on the bulk modulus for the previous studies of ice I_h, it is evident that the bulk modulus increases with decreasing temperature. This behaviour is seen in the present study - as temperature is decreased the bulk modulus of ice increases. The cause for such

differences between the bulk modulus obtained in this work and those obtained by previous studies is likely the glycoproteins in the mucus altering the size, shape, and possibly even the composition, of the ice crystals [48].

4.4 Sound Absorption - Temperature Dependence

Tables 4.1 - 4.3 give the tabulated values for full width at half maximum (FWHM) of both the mucus and ice peak for each sample. The FWHM was obtained by fitting a Lorentzian function to each Brillouin peak and averaging the peak width for the Stokes and anti-Stokes peaks. In addition, the instrumental linewidth was measured to be $\sim$ 0.3 GHz and was subtracted from linewidth values obtained from the Lorentzian fit to remove its contribution to the FWHM. The uncertainty in the FWHM comes from uncertainty in the Lorentzian fit. Appendix A gives the python code used for the Lorentzian fit.

Figures 4.14 - 4.16 show the FWHM of both the mucus peak and the ice peak as functions of temperature for all samples studied in this work. For temperatures greater than T = -2.5°C, it is evident that the FWHM of the mucus peak decreases exponentially with increasing temperature. Below this temperature the rate of decay is different, but the linewidth still displays an exponential decrease. It is expected that the FWHM of the mucus mode should exponentially change as a function of temperature since the linewidth is directly proportional to the liquid viscosity which is of the form $\eta = A\exp(B/T)$ [49]. Values obtained for the FWHM change from $\sim$ 6.0 GHz at T = -2.5 °C to $\sim$ 0.7 GHz at T = 50°C. In contrast, the FWHM of the ice mode remains constant at $\sim$ 0.6 GHz for all temperatures below T = -2.5°C.

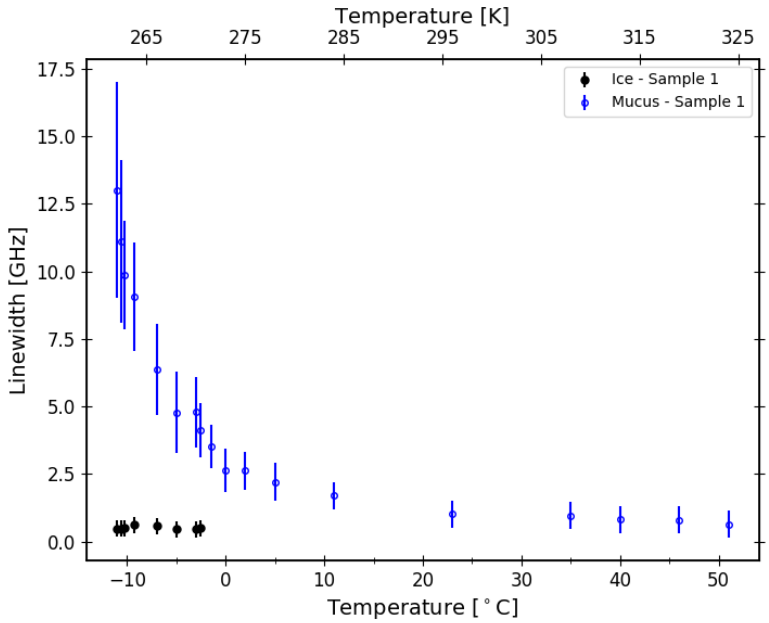

Figure 4.14: FWHM versus temperature for gastropod mucus - Sample 1. ○ - Mucus mode, ● - Ice mode.

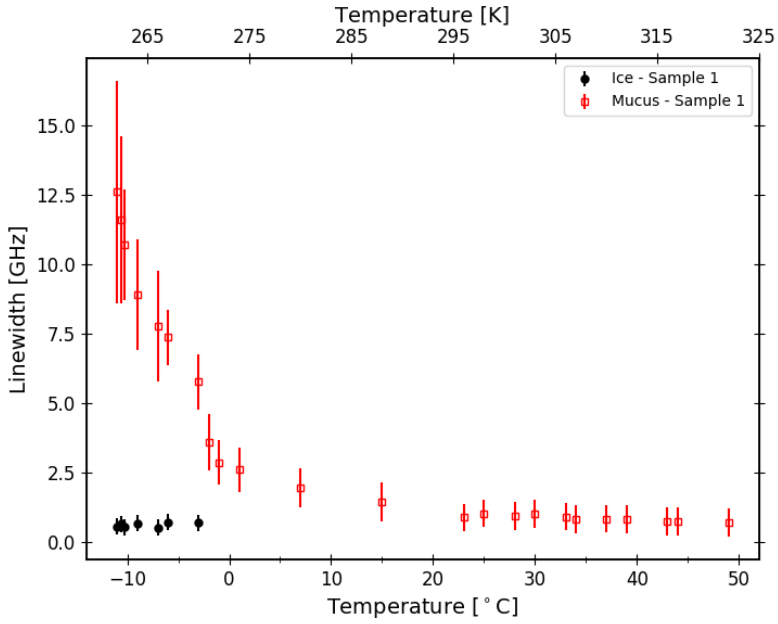

Figure 4.15: FWHM versus temperature for gastropod mucus - Sample 1. □ - Mucus mode, ■ - Ice mode.

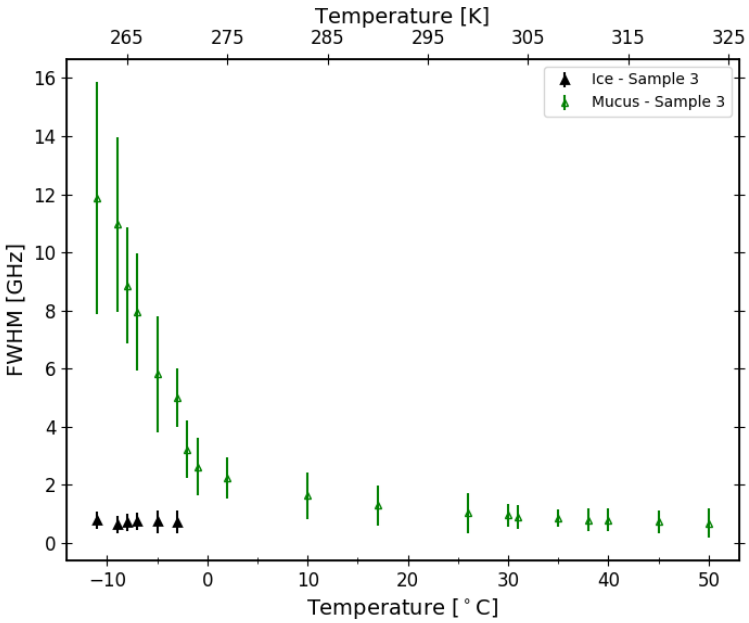

Figure 4.16: FWHM versus temperature for gastropod mucus - Sample 1. △ - Mucus mode, ▲ - Ice mode.

Brillouin scattering on water with different concentrations of salt has been studied over a temperature range of 0°C ≤ T ≤ 40°C [45]. Salt water was used here for comparisons due to the fact that there are salt ions comprising some percentage of the mixture. Pure water is also discussed here and compared to both salt water and mucus. Results from that study showed that the FWHM of the water peak decreased exponentially as the temperature was increased for both normal pure water and water with a 35% salt concentration. The FWHM of the pure water peak had values of 1.4 GHz at T = 0°C and 0.6 GHz at T = 35°C. Similarly, the FWHM of the peak obtained for water with a salinity of 35% had values of 1.7 GHz at T = 0°C and 0.6 GHz at T = 35°C. These values are very similar to the FWHM values obtained for the mucus peak in the present work: ∼ 2.6 GHz at T = 0°C and 1.0 GHz at T = 35°C. This indicates that the addition of a solvent (salt in this case) increases the sound absorption. The FWHM at temperatures up to $T \sim 40$°C for water peaks are

very similar to values of FWHM obtained for mucus peaks presented in this work. At lower temperatures, the FWHM of the mucus and pure water peaks show a difference of approximately 47 % at T = 0°C, likewise a difference of 38% is observed between mucus and water with a 35% salt concentration at this temperature. The behaviour of the FWHM as a function of temperature for the mucus peak and for the peak due to water with a concentration of 35% both increase at a greater rate for lower temperatures as compared to pure water. This is evident from the relative values of FWHM at T = 0°C and T = 35°C.

The sound absorption (α/f^2) for the mucus mode as a function of temperature was calculated using Eqn. 2.34 which relies on the Brillouin peak linewidths (FWHMs), the frequency shifts recorded in Tables 4.1 - 4.3, and the phonon velocities tabulated in Table 4.4. The uncertainty in the sound absorption was calculated using standard error analysis formulae with uncertainties in FWHM, frequency shift, and sound velocity. The ice mode will not be considered in this analysis since its velocity and the FWHM of the associated spectral peak remain relatively constant over the full temperature range.

The sound absorption as a function of temperature is recorded in Table 4.6 and is shown in Figures 4.17 - 4.19. In general, the temperature dependence of the sound absorption is similar for all samples studied over the entire temperature range. Values over the temperature range 15°C - 50°C were found to be $\sim$ 5 - 10 $\times 10^{-15} s^2$/m. For temperatures below T = 15°C the sound absorption exponentially increases until T = -2.5°C where the value is $\sim$ 35 $\times 10^{-15} s^2$/m and an obvious change in the temperature dependence occurs. Below T = -2.5°C the sound absorption continues to increase exponentially (at a different rate) with decreasing temperature. The sound absorption increases from 35 $\times 10^{-15}$s^2/m at T = -2.5 °C to 100 $\times 10^{-15}$ s^2/m at T = -11.0 °C. The maximum value obtained for each sample is $\sim$ 100 $\times 10^{-15}$s^2/m which occurs at

T = -11.0 °C. Previous studies for the sound absorption in water show that sound absorption increases with decreasing temperature, much like what is observed in the present study [27–30, 32], however there is no prior evidence of an anomaly at T = -2.5 °C.

Table 4.6: Sound absorption (α/f^2) calculated for the liquid phase of gastropod mucus for Samples 1, 2 and 3 using Equation 2.34.

Sample 1			Sample 2			Sample 3		
T [$\pm$ 0.5 K]	T [$\pm$0.5°C]	α/f^2 [10^{-15}s^2/m]	T [$\pm$ 0.5 K]	T [$\pm$0.5°C]	α/f^2 [10^{-15}s^2/m]	T [$\pm$0.5K]	T [$\pm$0.5°C]	α/f^2 [10^{-15}s^2/m]
324.0	51.0	4 ± 2	322.0	49.0	6 ± 4	323.0	50.0	6 ± 4
319.0	46.0	6 ± 4	317.0	44.0	7 ± 4	318.0	45.0	7 ± 4
313.0	40.0	6 ± 4	316.0	43.0	7 ± 4	313.0	40.0	7 ± 4
308.0	35.0	7 ± 4	312.0	39.0	8 ± 5	311.0	38.0	7 ± 3
296.0	23.0	7 ± 3	310.0	37.0	8 ± 5	308.0	35.0	8 ± 4
284.0	11.0	13 ± 4	307.0	34.0	9 ± 4	304.0	31.0	8 ± 3
278.0	5.0	18 ± 6	306.0	33.0	10 ± 4	303.0	30.0	9 ± 4
275.0	2.0	23 ± 7	303.0	30.0	8 ± 4	298.0	25.0	10 ± 5
273.0	0.0	22 ± 8	301.0	28.0	9 ± 4	290.0	17.0	12 ± 7
272.0	-1.5	32 ± 9	298.0	25.0	9 ± 4	283.0	10.0	16 ± 8
271.0	-2.5	40 ± 10	296.0	23.0	8 ± 4	275.0	2.0	22 ± 8
270.0	-3.0	40 ± 10	288.0	15.0	14 ± 6	272.0	-1.0	30 ± 10
268.0	-5.0	30 ± 10	280.0	7.0	20 ± 8	271.0	-2.5	30 ± 10
266.0	-7.0	40 ± 10	274.0	1.0	30 ± 10	270.0	-3.0	50 ± 10
264.0	-9.3	50 ± 10	272.0	-1.0	30 ± 10	268.0	-5.0	50 ± 20
263.0	-10.3	60 ± 10	271.0	-2.5	40 ± 10	266.0	-7.0	70 ± 20
262.0	-10.6	70 ± 20	270.0	-3.0	60 ± 10	265.0	-8.0	70 ± 30
262.0	-11.0	100 ± 30	267.0	-6.0	70 ± 10	264.0	-9.0	90 ± 30
			266.0	-7.0	60 ± 20	262.0	-11.0	100 ± 40
			264.0	-9.3	70 ± 20			
			263.0	-10.3	80 ± 20			
			262.0	-10.6	90 ± 30			
			262.0	-11.0	110 ± 40			

In Figures 4.17 - 4.19, it is clear that the temperature dependence of the sound absorption is different for temperatures above and below T = -2.5°C. It is possible to fit both regions to exponential functions of the form $\frac{\alpha}{f^2} = A\exp(B/T)$, as described above where A and B are fit parameters which are tabulated in Table 4.7. The temperature dependence of α/f^2 is a typical Arrhenius behaviour [49]. Recall from Chapter 2 that the sound absorption is proportional to the FWHM which is proportional to viscosity, $\eta = A\exp\left(\frac{\epsilon}{k_B T}\right)$, where k_B is the Boltzmann constant and ϵ is a measure of the strength of interaction between molecules comprising the liquid, also referred to as an activation energy [49]. Comparing the functions for α/f^2 and for η it can be seen that the exponential term B is equal to ϵ/k_B and the interaction energy, ϵ can be found by rearranging this equation. Values calculated for ϵ are recorded in Table 4.7.

Considering now the values from Table 4.7, the values of A both above and below T = -2.5°C are consistent throughout this study with values on the order of $\sim 10^{-20}$ s^2K/m. The factor B in the exponent is also consistent for temperatures above and below T = -2.5 °C with values on average $\sim$ 3900 $\pm$ 500 s^2K/m. Likewise, for temperatures below T = -2.5°, the factor B increases to a value about of $\sim$ 7600 $\pm$ 600 s^2K/m. Since the factor B in the exponent is related to the interaction between molecules in the liquid, it makes sense that below T = -2.5°C the factor B be greater than for temperatures above T = -2.5°C due to the solid ice crystals present in the mucus. Similarly, as a result of the ice growth, there is likely a higher concentration of glycoproteins in the liquid phase of the mucus which would result in a change of its acoustic properties. The interaction energy between molecules in mucus was calculated for temperatures above and below T = -2.5°C. Results of this calculation yielded an energy of $\sim 5.2 \times 10^{-20}$J for temperatures above T = -2.5°C. Similarly for T $\leq$ -2.5°C, the interaction energy was found to be $\sim 10.4 \times 10^{-20}$J.

Table 4.7: Best-fit parameters for fit of function $\alpha/f^2 = A\exp(B/T)$ to experimental sound absorption data for temperatures above and below T = -2.5°C.

Temperature	Sample	$A \times 10^{-20}$ s^2/m	$B \times 10^3$ s^{2}K/m	$\epsilon \times 10^{-20} J$
-2.5 °C $\leq$ T $\leq$ 52.0 °C	1	1.1 ± 0.9	4.7 ± 0.5	6.5 ± 0.9
	2	3.1 ± 0.8	3.6 ± 0.6	4.9 ± 0.7
	3	2.8 ± 0.7	3.3 ± 0.5	4.3 ± 0.7
-11.0 °C $\leq$ T $\leq$ -2.5 °C	1	8.7 ± 0.9	9.2 ± 0.9	12.4 ± 0.9
	2	4.4 ± 0.9	6.9 ± 0.3	9.5 ± 0.7
	3	4.6 ± 0.7	6.8 ± 0.8	9.4 ± 0.8

Previous studies on the viscosity water found the activation energy to be about $\sim 2.6 \times 10^{-20}$J [50] for temperatures over the range 10°C $\leq$ T $\leq$ 20°C. The activation energy obtained in the current study are similar to the energies obtained for water. The fact that the interaction energy for mucus is greater than that of water is not surprising. First of all, the FWHM is greater for mucus than for water as was previously seen, indicating that the viscosity is greater (see Eqn 2.34). As well, the presence of glycoproteins in the mucus add another interaction between water molecules in the mucus which would require more energy.

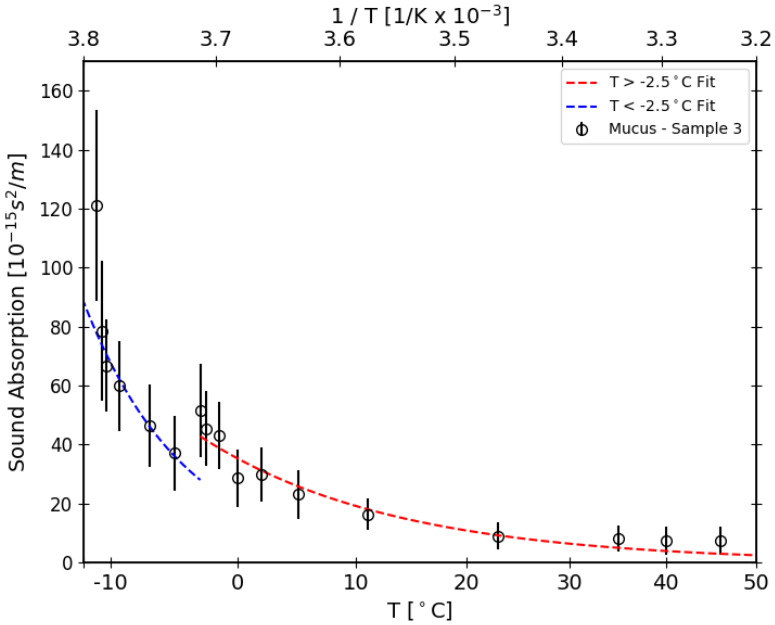

Figure 4.17: Sound absorption inferred Brillouin peaks for Sample 1 as a function of temperature. ○ - Mucus peaks.

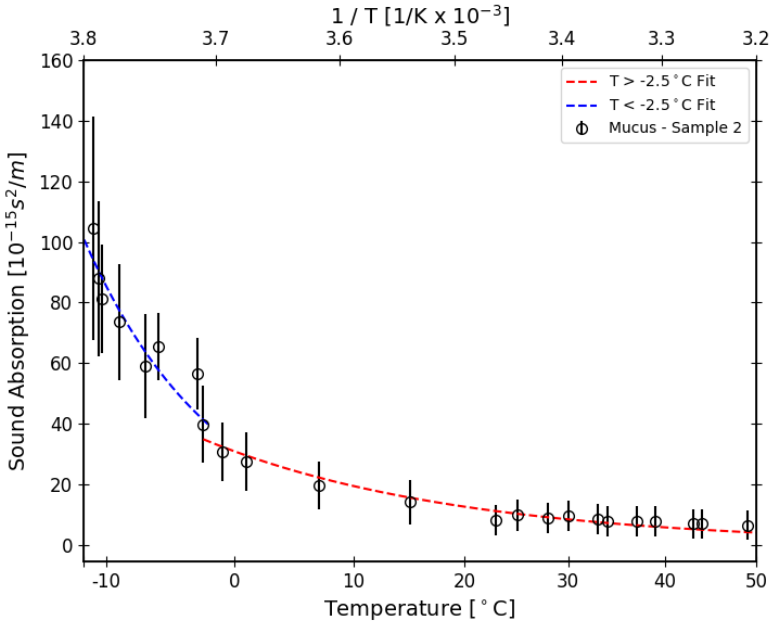

Figure 4.18: Sound absorption inferred Brillouin peaks for Sample 2 as a function of temperature. ○ - Mucus peaks.

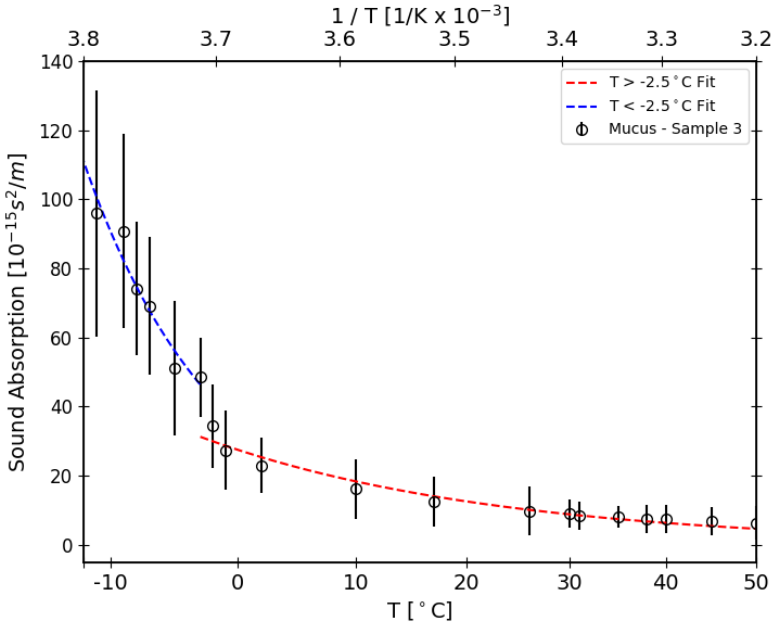

Figure 4.19: Sound absorption inferred Brillouin peaks for Sample 3 as a function of temperature. ○ - Mucus peaks.

The sound absorption in water was previously obtained and showed an exponential increase as temperatures decreased [29, 30, 32]. At T = 0°C the sound absorption in water was approximately $40\times10^{-15}s^2$/m [29,30] when obtained by Brillouin scattering. A value of 137 $\times10^{-15}$ s^2/m was obtained by ultrasonics [32]. For T = -2.5 °C, the sound absorption for the mucus mode is $\sim 25\times10^{-15}s^2$/m which is 50 % of the value of 50 $\times10^{-15}s^2$/m obtained for water by Brillouin scattering. However, the sound absorption at -10°C for water and mucus both had values of $75\times10^{-15}s^2$/m [29,30]. In order for this to happen the sound absorption would need to increase more quickly for mucus at lower temperature since the values differed so much for higher temperatures. Both mucus and water display the largest damping at colder temperatures.

The sound absorption was found for similar liquids, particularly mixtures of glycerol-water [26] and polyvinylpyrrolidone-water [28] by ultrasonic techniques, as well for polyethylene glycol [27] by Brillouin scattering. The results for the sound absorption

of water with a 15% glycerol concentration shows that as temperature increases the sound absorption increases over the temperature range 0°C $\leq$ T $\leq$ 50°C which is opposite to the present work. This increase is true for concentrations up to 80% glycerol. The sound absorption of polyethylene glycol (PEG) and water with a 5% PEG concentration was obtained and showed a decrease in sound absorption with increasing temperature over range 280K $\leq$ T $\leq$ 360K which is similar to what is found in this work. The sound absorption for polyethylene glycol-water mixture varies between 0.3 - 0.8$\times 10^{-15}$ s^2/m which is about 100 times smaller than the sound absorption for the mucus mode. As well the values of sound absorption for polyethylene glycol, 0.7$\times 10^{-15}$ s^2/m, and mucus, 15$\times 10^{-15}$ s^2/m, differ by more than 2000 % at T = 30 °C. The cause for such difference is unknown and further studies are required. Sound absorption for a solution of polyvinylpyrrolidone(PVP)-water [28] was obtained over the temperature range 20°C $\leq$ T $\leq$ 45°C. The values obtained for a solution of water consisting of 5% polyvinylpyrrolidone showed a nonlinear decrease in sound absorption for increasing temperature much like what has been observed for mucus with values ranging from 55$\times 10^{-15} s^2/m$ at T = 0°C to 35 $\times 10^{-15} s^2/m$ at T = 45°C. The values for mucus over the same temperature range were found to be 22$\times 10^{-15} s^2/m$ at T = 0°C and 6 $\times 10^{-15} s^2/m$ at T = 45°C, which are smaller than the values obtained for the PVP-water mixture. The sound absorption for both polyvinylpyrrolidone-water and mucus did show that as temperature increased the absorption also decreased and shows a trend consistent with that obtained previously for water and PEG-water [27, 29, 30].

4.5 Peak Intensity - Temperature Dependence

Peak intensities and associated uncertainties at different temperatures were obtained by fitting a Lorentzian function to each Brillouin peak. These values are tabulated in

Tables 4.1 - 4.3 and plotted in Figures 4.20 - 4.22. Although there is some scatter in the data (particularly for Sample 1, but also for Sample 2), it can be seen that the mucus peak intensity decreases roughly linearly as the temperature decreases from $T = 50°C$ to $T \sim 0°C$. For temperatures in the range $-2.5 \leq T \leq 0°$, a linear decrease of intensity with temperature was also observed, but the rate of decrease is significantly greater than that seen in the higher temperature range. For $-11.0°C \leq T \leq -2.5°C$, the intensity of the mucus peak shows no particular dependence on temperature but, overall, shows a decrease from $\sim$ 4000 counts at T = -2.5 °C to $\sim$ 300 at T = -11.0 °C. Interestingly, over this same temperature range, the intensity of the ice peak increases with decreasing temperature. These trends in the mucus and ice peak intensities over this temperature range likely indicates that more ice is forming in the sample as the temperature is decreased.

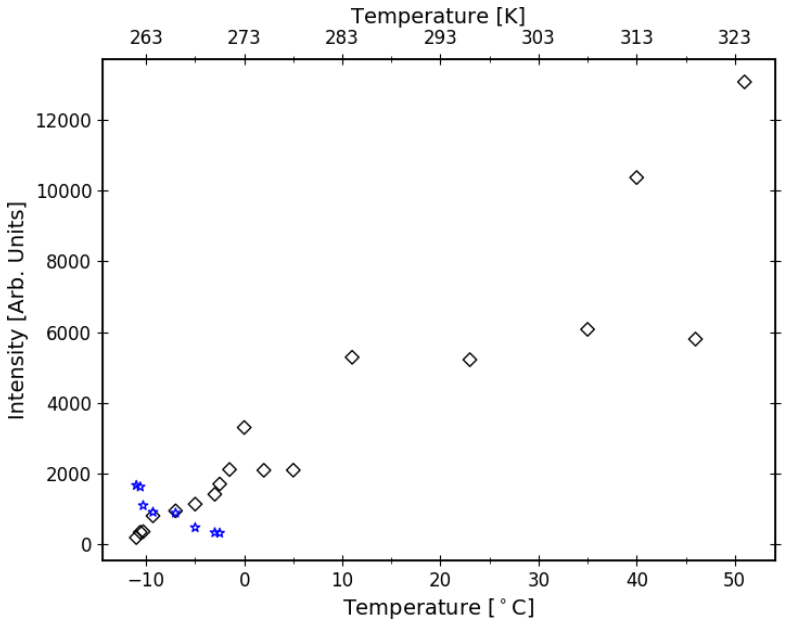

Figure 4.20: Brillouin peak intensity for gastropod mucus Sample 1. ◊ - Mucus peak, ⋆ - Ice peaks.

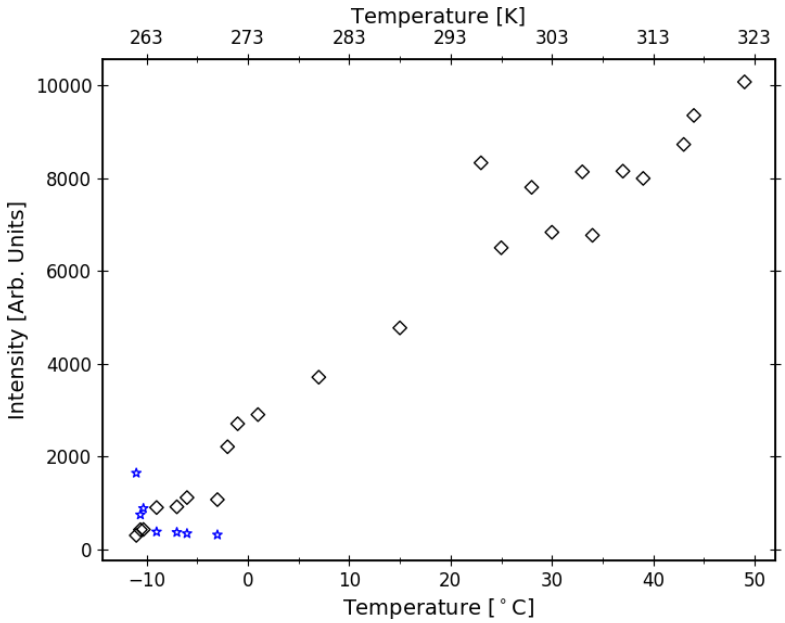

Figure 4.21: Brillouin peak intensity for gastropod mucus Sample 2. ◊ - Mucus peak, ⋆ - Ice peaks.

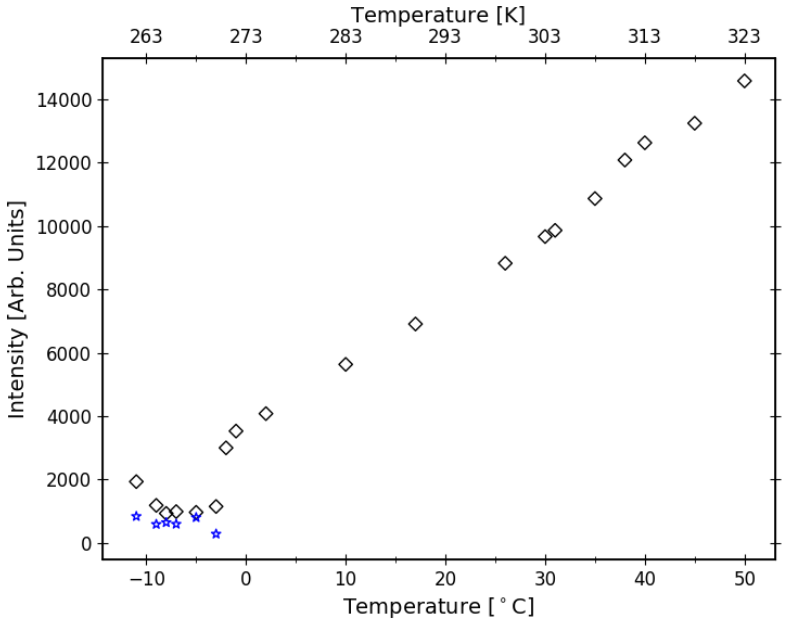

Figure 4.22: Brillouin peak intensity for gastropod mucus Sample 3. ◊ - Mucus peak, ⋆ - Ice peaks.

4.6 Phase Transition

Figure 4.24 shows a composite plot of intensity, sound absorption and sound velocity as a function of temperature for all samples studied. It is evident that all of these quantities display anomalous changes in behaviour at $T = -2.5°\text{C}$, as has been discussed in detail in Sections 4.2 - 4.5. When considered collectively, the above behaviours provide strong evidence for the existence of a phase transition from a wholly liquid phase to a solid-liquid phase at a temperature of $T = -2.5°\text{C}$. The similarities between the results obtained in the present work and results obtained for previous studies on water, and other similar liquids suggest that above T = -2.5°C the mucus is behaving as a wholly liquid.

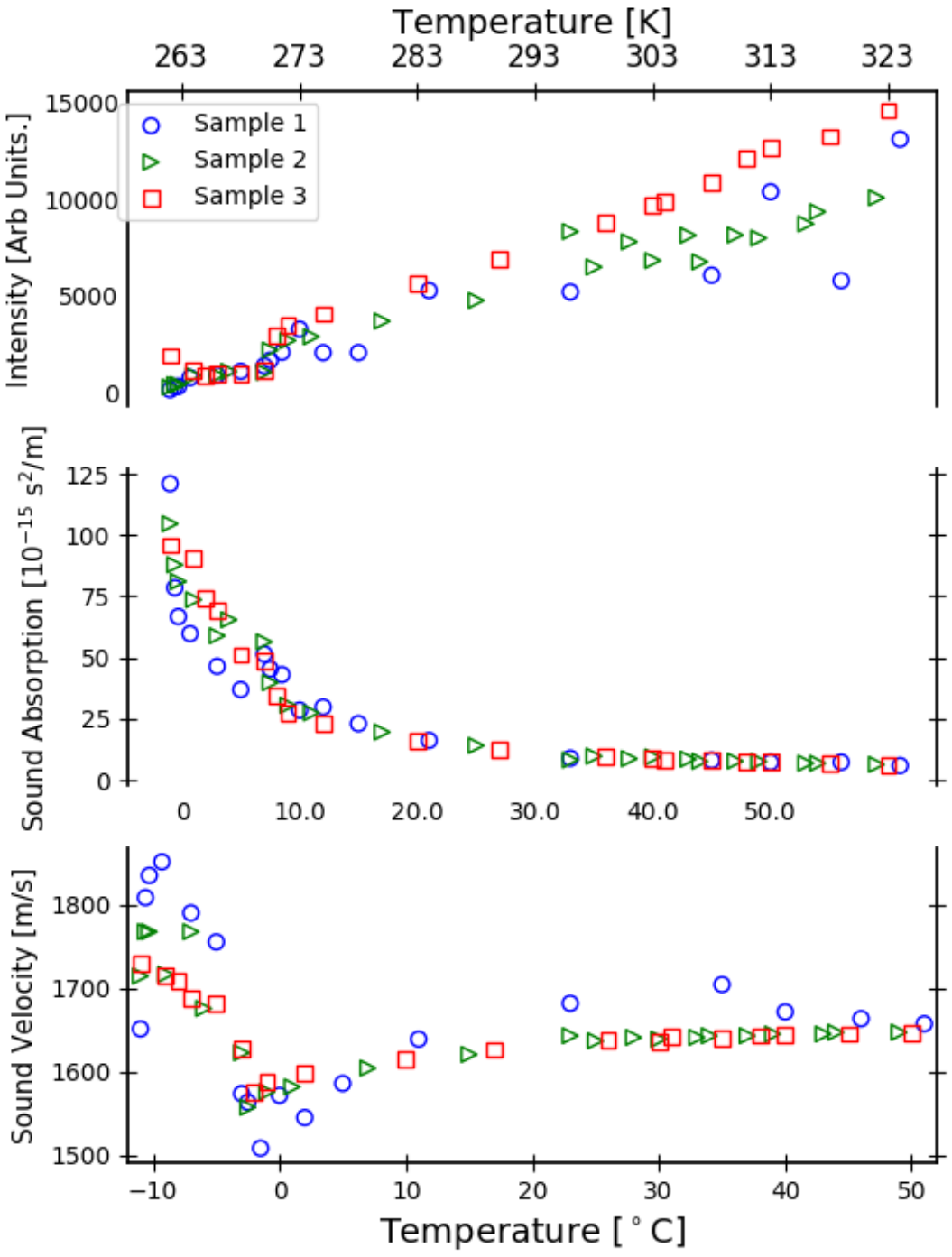

Figure 4.23: Sound velocity, sound absorption and Brillouin peak intensity versus temperature for gastropod mucus of all samples. Vertical dashed line represents a transition from a wholly liquid phase to a solid-liquid phase.

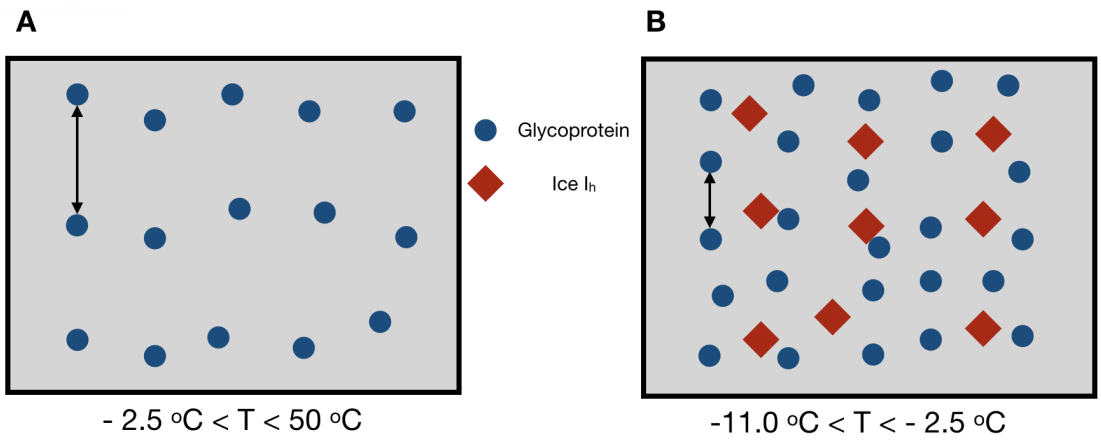

Figure 4.24: Schematic showing the two known phases of gastropod mucus A) Wholly liquid phase for the temperature regime -2.5°C $\leq$ T $\leq$ 50°C, B) Solid-liquid phase for the temperature regime -11.0°C $\leq$ T $\leq$ -2.5°C.

Figure 4.24 gives a schematic representation of what appears to be happening in the mucus. Considering the temperature region -2.5°C $\leq$ T $\leq$ 52°C as the mucus is behaving as a wholly liquid as is shown in Fig 4.24 A. In this diagram the molecules of the mucus are relatively far apart, as is the case for a normal liquid such as water. The results obtained throughout this work for temperatures greater than T = -2.5°C are similar to the results obtained for water and related liquids, indicating that the mucus is in fact in a wholly liquid phase.

Considering now the temperature regime -11.0°C $\leq$ T $\leq$ -2.5°C as shown in Fig 4.24 B, the properties of the mucus are different than those obtained above T = -2.5°C. Below this temperature the liquid mucus is still present. As well, in this temperature regime there is the presence of ice in the mucus which has been described previously. The results from this work suggest the coexistence of both the liquid mucus and solid ice phases below T = -2.5°C as shown in Fig 4.24 B. As well, there is evidence that as the temperature decreases there is more ice forming, excluding the glycoproteins, which further supports the conclusion of the coexistence of both liquid mucus and solid ice phases. There is further evidence that as these phases coexist the liquid

mucus has become water-depleted since some of the water which was originally in the liquid phase has solidified to ice. Finally, the fact that the mucus peak intensity decreases with decreasing temperature while the ice peak intensity increases, suggests a completion of the phase transition to solid ice at a lower temperature than that studied.

Chapter 5

Conclusion

5.1 Summary

Brillouin light scattering was used to investigate the effects of temperature on acoustic phonons in natural gastropod mucus. For temperatures greater than -2.5°C a single peak due to liquid mucus showed a large temperature dependence in the acoustic properties as a function of temperature. For temperatures below -2.5°C two peaks were observed one of which was the same liquid mucus peak, the other peak was due to ice . The peak due to ice was observed at a frequency shift of approximately 18.5 GHz and showed slight changes over the temperature range studied. The frequency shift of the mucus peak was used to obtain the acoustic velocities and consequently the bulk modulus as a function of temperature. Moreover, the mucus peak intensity showed a linear increase with increasing temperature for temperatures greater than T = -2.5°, but an overall decrease in intensity for temperatures below T = -2.5°. The full width at half maximum of the mucus Brillouin peaks was used in accordance with the phonon velocity and frequency shift to obtain the sound absorption (α/f^2) as a function of temperature. Results for the sound absorption yielded values for the

activation energy for molecular transport in the mucus which were comparable to the values for water.

Furthermore, the frequency shift of the ice peak was used to obtain the acoustic velocities of ice as a function of temperature. Results showed that the velocity increased slightly as temperature decreased. The bulk modulus of ice showed the same trend as a function of temperature as the phonon velocity. Moreover, the peak intensity of the ice peak increased as temperature decreased. The FWHM of the ice peak remained essentially constant over the full temperature range.

Collectively, the results of this work indicate that slug mucus undergoes a phase transition from a wholly liquid phase to a solid-liquid phase at T = -2.5°C. Moreover, as temperature is decreased below -2.5°C, more ice forms in the mucus.

5.2 Future Work

The results of the present study suggest that the presence of glycoproteins in water greatly influences its acoustic properties. To fully understand the true nature of these glycoproteins and their behaviour, however, additional studies over different temperature regimes are necessary. It would also be interesting to do studies similar to that of the present work but vary other parameters such as pH, pressure, and hydration state to obtain more information on mucus elasticity. Furthermore, studies on other natural materials (such as other types of gastropod mucus, fluids containing antifreeze proteins from cold water fish, etc.) would be interesting and would contribute to our understanding of the elasticity of such materials.

Appendix A

Python Code for Lorentzian Fit

Python code used to fit a Lorentzian function to Brillouin peaks. From the Lorentzian fit, it is possible to obtain the Brillouin peak intensity, full width at half maximum and the frequency shift. In the code below, the term "A" represents the peak intensity, "wid" represents the full width at half maximum and "x0" represents the frequency shift.

```
import numpy as np
import matplotlib.pyplot as plt
import sys
from lmfit import Model
#Insert File of Brillouin Spectra
dat_1 = np.genfromtxt('Mucus_Sample4 24022020 2.TXT',delimiter=' ')


xf = dat_1[:,0] # Full X Range
# Lower Shift on LHS   x data  for mucus peaks :300:460 / for ice peaks
x1 = dat_1[200:310,0]
```

```
# Lower Shift on RHS   x data  for mucus peaks :564:724 / for ice peaks
x2 = dat_1[694:824,0]

yf = dat_1[:,1] # Full Y Range
y1 = dat_1[200:310,1] # Lower Shift on LHS   y data
y2 = dat_1[694:824,1] # Lower Shift on RHS   y data

def lorentz(x, y0, A, x0, wid): # Function
    """Fit =y0+(2*A/pi).*(w./(4*(x x0).^2+w.^2))"""
    return (y0 + A * wid / (4*(x x0)**2 + wid**2))

gmodel = Model(lorentz)
result1 = gmodel.fit(y1, x=x1,y0 = 1200, A=5000, x0=9.5, wid= 3.5) # LHS
result2 = gmodel.fit(y2, x=x2,y0 = 1200, A=5000, x0=9.5, wid=3.5) # RHS



print(result1.fit_report())
print(result2.fit_report())

#print(result1.params['x0'])

xLeft_x0 = str(result1.params['x0'])  # Exrtact x0 LHS
xLeft_wid = str(result1.params['wid']) # Exrtact wid LHS
xLeft_I = str(result1.params['A'])  # Exrtact x0 LHS
xRight_x0 = str(result2.params['x0']) # Extract x0 RHS
xRight_wid = str(result2.params['wid']) # Extract wid RHS
```

```
xRight_I= str(result2.params['A']) # Extract x0 RHS


xleftx0 = float(xLeft_x0[24:34])
#xleftx0err = float(xLeft_x0[45:51])
#xleftI= float(xLeft_I[23:34])
###
xrightx0 = float(xRight_x0[23:33])
#xrightx0err = float(xRight_x0[45:51])
#xrightI = float(xRight_I[23:33])
####
xleftwid = float(xLeft_wid[24:35])
#xleftwiderr = float(xLeft_wid[46:51])
xrightwid = float(xRight_wid[24:35])
#xrightwiderr = float(xRight_wid[46:51])

Fshift = (xleftx0 + xrightx0)/2
#Fshifterr = (xleftx0err + xrightx0err)/2
FWHM = (xleftwid + xrightwid)/2
#FWHMerr = (xleftwiderr + xrightwiderr)/2
#Intensity =  (xleftI + xrightI)/2



Intensity = (np.amax(y1) + np.amax(y2))/2
print(Intensity)

## Output to TXT fild#
```

```
output = open("Intensity_Ice_Sample4.txt","a")
#output2 = open("FrequencyShift_S4.txt","a")

print(Intensity,file=output)
#print(Fshift,file=output2)
####

#print('Frequency Shift = ', Fshift, '+/ ', Fshifterr, 'GHz')
#print('FWHM =  ', FWHM,'+/ ',FWHMerr,'GHz')



#plt.plot(xf, yf, 'bo')
plt.plot(x1, y1, 'k ')
plt.plot(x2, y2, 'k ')
plt.plot(x1, result1.best_fit, 'r ', label='best fit')
plt.plot(x2, result2.best_fit, 'r ')
plt.legend(loc='best')
plt.xlim(25,25)
plt.ylim(0,9000)
#plt.savefig('test.png')
plt.show()
```

Bibliography

[1] P. Verdugo, I. Deyrup-Olsen, M. Aitken, M. Villalon, and D. Johnson. Molecular mechanism of mucin secretion: I. the role of intragranular charge shielding. *Journal of Dental Research*, 66(2):506–508, 1987.

[2] Y. Zhou, D. Huitink, and H. Liang. Lubrication behavior of slug mucus. *Materials Performance and Characterization*, 1(1):1–8, 2012.

[3] M. Campion. The structure and function of the cutaneous glands in helix aspersa. *Journal of Cell Science*, 3(58):195–216, 1961.

[4] J.M Pawlicki, L.B Pease, CM Pierce, T.P Startz, Y. Zhang, and A.M Smith. The effect of molluscan glue proteins on gel mechanics. *Journal of experimental biology*, 207(7):1127–1135, 2004.

[5] M.W Denny. Mechanical properties of pedal mucus and their consequences for gastropod structure and performance. *American Zoologist*, 24(1):23–36, 1984.

[6] R.G. Spiro. Glycoproteins. *Annual Review of Biochemistry*, 39(1):599–638, 1970.

[7] M.E . Taylor and K. Drickamer. *Introduction to Glycobiology.* Oxford University Press, 2011.

[8] J. Newar and A. Ghatak. Studies on the adhesive property of snail adhesive mucus. *Langmuir*, 31(44):12155–12160, 2015.

[9] J. Lechner and F. Wieland. Structure and biosynthesis of prokaryotic glycoproteins. *Annual Review of Biochemistry*, 58(1):173–194, 1989.

[10] P. Messner. Bacterial glycoproteins. *Glycoconjugate Journal*, 14(1):3–11, 1997.

[11] G. L. Fletcher, C. L. Hew, and P. L. Davies. Antifreeze proteins of teleost fishes. *Annual Review of Physiology*, 63(1):359–390, 2001.

[12] Y. Yeh and R. E. Feeney. Antifreeze proteins: Structures and mechanisms of function. *Chemical Reviews*, 96(2):601–618, 1996.

[13] C. L. Hew, D. Slaughter, S. B. Joshi, G. .L Fletcher, and V. S. Ananthanarayanan. Antifreeze polypeptides from the newfoundland ocean pout, macrozoarces americanus: presence of multiple and compositionally diverse components. *Journal of Comparative Physiology B*, 155(1):81–88, 1984.

[14] C. L. Hew, D. Slaughter, G. L. Fletcher, and S. B. Joshi. Antifreeze glycoproteins in the plasma of newfoundland atlantic cod (gadus morhua). *Canadian Journal of Zoology*, 59(11):2186–2192, 1981.

[15] S. Venketesh and C. Dayananda. Properties, potentials, and prospects of antifreeze proteins. *Critical Reviews in Biotechnology*, 28(1):57–82, 2008.

[16] T. Dojima, T. Nishina, T. Kato, T. Uno, H. Yagi, K. Kato, and E. Y. Park. Comparison of the n-linked glycosylation of human β1, 3-n-acetylglucosaminyltransferase 2 expressed in insect cells and silkworm larvae. *Journal of Biotechnology*, 143(1):27–33, 2009.

[17] A. J. Pietrzyk, A. Bujacz, P. Mak, B. Potempa, and T. Niedziela. Structural studies of helix aspersa agglutinin complexed with galnac: a lectin that serves as

a diagnostic tool. *International Journal of Biological Macromolecules*, 81:1059–1068, 2015.

[18] R. Strasser, F. Altmann, and H. Steinkellner. Controlled glycosylation of plant-produced recombinant proteins. *Current Opinion in Biotechnology*, 30:95–100, 2014.

[19] K. V. Lithgow, N. E. Scott, J. A. Iwashkiw, E. Thomson, L. J. Foster, M. F. Feldman, and J. J. Dennis. A general protein o-glycosylation system within the b urkholderia cepacia complex is involved in motility and virulence. *Molecular Microbiology*, 92(1):116–137, 2014.

[20] L. L. Lovelace, C. L. Cooper, J. M. Sodetz, and L. Lebioda. Structure of human c8 protein provides mechanistic insight into membrane pore formation by complement. *Journal of Biological Chemistry*, 286(20):17585–17592, 2011.

[21] A. E. Aleshin, I. U. Schraufstatter, B. Stec, L. A. Bankston, R. C. Liddington, and R. G. DiScipio. Structure of complement c6 suggests a mechanism for initiation and unidirectional, sequential assembly of membrane attack complex (mac). *Journal of Biological Chemistry*, 287(13):10210–10222, 2012.

[22] A.M. Smith. The structure and function of adhesive gels from invertebrates. *Integrative and Comparative Biology*, 42(6):1164–1171, 2002.

[23] J Stefan. Versuche über die scheinbare adhäsion. *Annalen der Physik*, 230(2):316–318, 1875.

[24] L. D. Landau and E. M. Lifshitz. Fluid mechanics. 1959. *Course of theoretical physics*, 1959.

[25] A.M. Wilks, S.R. Rabice, H.S. Garbacz, C.C. Harro, and A.M. Smith. Double-network gels and the toughness of terrestrial slug glue. *Journal of Experimental Biology*, 218(19):3128–3137, 2015.

[26] G. S. Darbari, R. P. Sinsgh, and G. S. Verma. Temperature dependence of ultrasonic absorption in mixtures of glycerol and water. *Il Nuovo Cimento B (1965-1970)*, 41(1):15–24, 1966.

[27] M. Pochylski, F. Aliotta, Z. Blaszczak, and J. Gapiński. Structuring effects and hydration phenomena in poly(ethylene glycol)/water mixtures investigated by Brillouin scattering. *The Journal of Physical Chemistry B*, 110(41):20533–20539, 2006.

[28] P. Spickler, I. Abdel-Raziq, S. Yun, and F. B. Stumpf. Velocity and absorption of ultrasound in binary solutions of polyvinylpyrrolidone and water. *The Journal of the Acoustical Society of America*, 85(3):1363–1364, 1989.

[29] J. Rouch, C. C. Lai, and S. H. Chen. Brillouin scattering studies of normal and supercooled water. *The Journal of Chemical Physics*, 65(10):4016–4021, 1976.

[30] J. Teixeira and J. Leblond. Brillouin scattering from supercooled water. *Journal de Physique Lettres*, 39(7):83–85, 1978.

[31] C. L.. O'Connor and J. P Schlupf. Brillouin scattering in water: the landau—placzek ratio. *The Journal of Chemical Physics*, 47(1):31–38, 1967.

[32] F. E. Fox and G. D. Rock. Compressional viscosity and sound absorption in water at different temperatures. *Physical Review*, 70(1-2):68, 1946.

[33] R. E. Gagnon, H. Kiefte, M. J. Clouter, and E. Whalley. Acoustic velocities and densities of polycrystalline ice ih, ii, iii, v, and vi by Brillouin spectroscopy. *The Journal of Chemical Physics*, 92(3):1909–1914, 1990.

[34] PH Gammon, H Kiefte, and MJ Clouter. Elastic constants of ice by Brillouin spectroscopy. *Journal of Glaciology*, 25(91):159–168, 1980.

[35] P. H. Gammon, H. Kiefte, and M. J. Clouter. Elastic constants of ice samples by Brillouin spectroscopy. *The Journal of Physical Chemistry*, 87(21):4025–4029, 1983.

[36] J. Li, A. D. Celiz, J. Yang, Q Yang, I. Wamala, W. Whyte, B. R. Seo, N. V. Vasilyev, J. J. Vlassak, and Z. Suo. Tough adhesives for diverse wet surfaces. *Science*, 357(6349):378–381, 2017.

[37] A.M. Polomska. *Brillouin Light Scattering from Carbon Nanotube Arrays*. PhD thesis, Memorial University of Newfoundland, 2005.

[38] L. Brillouin. Diffusion of light and x-rays by a transparent homogeneous body. *Ann. Phys*, 17(2):88–122, 1922.

[39] G. Benedek and T. Greytak. Brillouin scattering in liquids. *Proceedings of the IEEE*, 53(10):1623–1629, 1965.

[40] I. E. Morgan. *Brillouin Scattering Studies in Simple Liquids, Oxygen and Nitrogen*. PhD thesis, Memorial University of Newfoundland, 1976.

[41] B.J. Berne and R. Pecora. *Dynamic Light Scattering: with Applications to Chemistry, Biology, and Physics*. Courier Corporation, 2000.

[42] R Mauri. *Transport phenomena in multiphase flows*, volume 112. Springer, 2015.

[43] S. J. Spencer. Phonon dynamics of ceramic $pbsc_{0.5}ta_{0.5}o_3$. Master's thesis, Memorial University of Newfoundland, Canada, 2016.

[44] A. Yariv and P. Yeh. *Photonics: Optical Electronics in Modern Communications: Sixth Edition*. Oxford University Press Oxford, UK:, 2007.

[45] J. Xu, X. Ren, W. Gong, R. Dai, and D. Liu. Measurement of the bulk viscosity of liquid by Brillouin scattering. *Applied Optics*, 42(33):6704–6709, 2003.

[46] N. E. Dorsey. *Properties of Ordinary Water-Substance in all its Phases: Water-Vapor, Water, and all the Ices*. Number 81. Hafner Publishing Company, 1968.

[47] M. Mijaković, B. Kežić, L. Zoranić, F. Sokolić, A. Asenbaum, C. Pruner, E. Wilhelm, and A. Perera. Ethanol-water mixtures: Ultrasonics, Brillouin scattering and molecular dynamics. *Journal of Molecular Liquids*, 164(1-2):66–73, 2011.

[48] Y. Furukawa, K. Nagashima, S. Nakatsubo, I. Yoshizaki, H. Tamaru, T. Shimaoka, T. Sone, E. Yokoyama, S. Zepeda, and T. Terasawa. Oscillations and accelerations of ice crystal growth rates in microgravity in presence of antifreeze glycoprotein impurity in supercooled water. *Scientific Reports*, 7:43157, 2017.

[49] R Jones. *Soft Condensed Matter*, volume 6. Oxford University Press, 2002.

[50] A. Toumi, N. Hafaiedh, and M. Bouanz. Thermodynamic properties of triethylamine+water liquid mixture from shear viscosity measurements. *Fluid Phase Equilibria*, 278(1-2):68–75, 2009.